2012-03-09

Metacalibration in Geometric Optimization

Donald C. Sampson
Brigham Young University - Provo

Metacalibration in Geometric Optimization

Donald Sampson

A thesis submitted to the faculty of
Brigham Young University
in partial fulfillment of the requirements for the degree of

Master of Science

Michael Dorff, Chair
Gary Lawlor
James Cannon

Department of Mathematics

Brigham Young University

April 2012

ABSTRACT

Metacalibration in Geometric Optimization

Donald Sampson
Department of Mathematics, BYU
Master of Science

A introduction to metacalibration methods and their application. This includes a new proof of the double bubble conjecture, new results in the area of equitent problems (isoperimetric problems with boundary), and comments on a mapping conjecture.

Keywords: isoperimetric, metacalibration, double bubble, equitent

ACKNOWLEDGMENTS

I would like to thank my two advisors, Gary Lawlor and Michael Dorff, and all the people who have worked with me: Rebecca Dorff, James Dilts, Brandon Wilson, Drew Johnson, Jacob Ros, Neil Steinburg, Renetta Birdsall, Jeff Wade, Abraham Frandsen, Xin Chen, Holly Arrowood, Payton Lindsay, Joan Madsen, Amber Verser, and Amy Hancock.

Contents

List of Figures

Part I

A Friendly Introduction

A Prelude

Do you remember the last time you played with soap bubbles? Have you noticed that they almost all look the same? In fact, nearly every bubble you blow will quickly form into a sphere. Even very large bubbles, if they last long enough before popping, will eventually turn into spheres. Sometimes, though, bubbles will bump into each other. If you have blown bubbles enough, you've probably seen a double bubble: a soap bubble that has two air pockets, with an interior surface separating them. In double bubbles, each bubble surface looks like part of a sphere. Why do soap bubbles always form spheres?

In recent years, mathematicians have been playing with soap bubbles too. Besides being a lot of fun, bubbles provide an interesting mathematical problem: Why do they always form the same shape? Internal cohesion in soapy water causes soap films to minimize surface tension. This same surface tension causes drops of water to bead up on a table rather than spread out. In a soap film, however, minimizing surface tension is equivalent to minimizing surface area. We can guess that soap bubbles are always round because spheres are the shapes that minimize surface area. This is true for single bubbles, but what about double bubbles, or even triple bubbles? Are those shapes surface area minimizing too?

Minimizing surface area is an example of a geometric optimization problem. As they play with bubbles, mathematicians are asking what shapes or structures have the least surface area. Several questions have been answered using calculus of variations, but many remain unanswered. Today, mathematicians are developing new methods to tackle this type of problem. We will look at metacalibration, a new approach to geometric optimization problems that, along with previous calibration methods, allows us to take on these unanswered problems.

Chapter 1

Geometric Optimization

1.1 Soap Films and Soap Bubbles

The earliest and most recognized soap bubble researcher was Belgian physicist Joseph Plateau. He first started researching bubbles and surface tension in 1840 when a servant dropped some oil into a mixture of water and alcohol. Plateau noticed that the oil surfaces formed perfect spheres, which led to extensive experiments with soap films. He noticed that when he dipped a wire frame into a soap solution, the result was a surface that appeared to minimize surface area. From his experiments, Plateau devised four rules about the shapes that soap films form:

1. Soap films are made of smooth surfaces.

2. The mean curvature of a piece of soap film is constant for any piece on the same soap film. This implies that soap films look like parts of spheres.

3. Soap films meet in groups of three, at angles of 120°. This edge is called a Plateau border.

4. Plateau borders meet in groups of four at angles of $\cos^{-1}(\frac{-1}{3}) \approx 109.47^\circ$ to form a vertex.

Any soap film not meeting these conditions is unstable will quickly evolve to one that does.

In the past few decades, Plateau's results have sparked a great deal of interest in the mathematical community. The first task was to prove that Plateau's rules were correct: that area-minimizing surfaces in $\mathbb{R}^3$ follow Plateau's Rules. Building on work of her advisor (and eventually husband) Fredrick Almgren, Jean Taylor finally proved Plateau correct in 1976 [23].

Interest in Plateau's work did not stop there, however. Two problems sprang from his study of soap films: the existence problem and the instance problem.

1.2 The Existence Problem

Given a particular set of conditions, (such as fixed boundary as in Plateau's case), is there a surface that minimizes area among all surfaces meeting these conditions?

The existence problem has been studied extensively in the framework of geometric measure theory. Using a generalization of manifolds called rectifiable currents, Herbert Federer, Frederick Almgren, Jean Taylor, Frank Morgan and others were able to prove the existence of an area-minimizing current in a wide variety of problems. Going further, they were also able to prove several regularity results about area-minimizing rectifiable currents. For many of these problems, they have shown that the area-minimizing solutions are actually unions of manifolds. For most problems, the question of existence has been answered in the affirmative.

1.3 The Instance Problem

If there is an area-minimizing surface for a particular instance of a problem, what is the area minimizing surface?

As geometric measure theory has shown the existence of a minimizer in many optimization problems, the natural next question is 'What is it?' How do we find the minimizing figure and how do we prove that it is area-minimizing? As opposed to the existence problem, the instance problem

is still largely an open one.

Approaches to solving the instance problem fall into two general categories: indirect and direct. Calculus of variations, an indirect method, has historically been the main approach to the instance problem. In my research, I have focused on calibration, a direct method, as a relatively new alternative in solving instance problems.

1.4 Calculus of Variations and Indirect Proofs

In the past, calculus of variations has dominated geometric optimization problems. The variational approach is a generalization of the optimization methods found in classical calculus. The general idea is to take a derivative, set it equal to zero, and solve for the set of critical points. These critical points are the set of surfaces of first variation zero with respect to area. We find the minimizer by isolating the local minimizers from this set (analogous to taking the second derivative) and finding the minimum from among these. Variational methods also have one more requirement: we need to prove the existence of a minimizer. Even if there are local minimizers, there might not be a global minimum. (This has been the major impetus behind efforts to solve the existence problem.)

The variational approach is of necessity an indirect one. By taking the first variation, each competitor is compared to those nearby, and only locally minimal competitors are compared to the global minimum. For example, suppose we are instead trying to find the tallest person in a crowded room. The indirect approach of calculus of variations is akin to finding everyone who is taller than the people next to them and then comparing heights of the 'locally tallest' individuals.

Variational methods have strengths and weaknesses. One strength is that first variation zero surfaces can give insight into what shapes are likely to be minimizers. In some problems, variational methods can also give short proofs for minimization when the set of first variation zero surfaces is small. One of this method's major drawbacks is that many problems have large or

complex sets of local minimizers. Even in problems where the minimizer is all but universally accepted, formulating a proof of global minimization in a large set of first variation zero manifolds can be all but impossible. Variational methods also encounter the problem of proving the existence of a minimizer. This requires the existence problem to be solved before any proof can be called complete.

While variational methods have had great success in a variety of problems, the difficulties of the approach have left many others unanswered.

1.5 Calibrations and Direct Proofs

Calibration arguments explore a new avenue of direct proof. Instead of comparing each competitor to those near it, we compare each competitor directly to the conjectured minimizer. Recalling our previous example, finding the tallest person in a crowded room by a direct method would be akin to starting with the person who we think is tallest, and comparing their height to each person in the room directly.

In calibration proofs, this comparison is made by means of an intermediate function. Suppose that there exists some function G such that for some surface Ω^*,

$$Area(\Omega^*) = G(\Omega^*) \leq G(\Omega) \leq Area(\Omega)$$

for all other competing surfaces Ω. Then it is simple to see that Ω^* is area minimizing. Calibration proofs all follow this basic format. This is generally accomplished by using a specialized integrand (the calibration) to define G that relates it to the area of a competitor.

Chapter 2

Calibration Methods in Optimization Proof

What is an Optimization Problem?

Optimization problems ask what object has the least or most of something. Life is full of optimization problems. Every day we find people looking for the shortest route to work, the most goods they can get for their money, or the cheapest place to buy their groceries. Mathematicaly, an optimization problem has two parts: a set of competitors and a real-valued function to compare them with. The set of competitors is the collection of objects on which you try to maximize, or minimize, the function. We denote the set of competitors for a given optimization problem by $\mathscr{C}$. We also define the *objective function* $P : \mathscr{C} \to \mathbb{R}$ by which we measure each competitor. For each competitor Ω in $\mathscr{C}$, $P(\Omega)$ is a real number representing the value to be minimized or maximized. We say that a particular competitor Ω^* in $\mathscr{C}$ minimizes P if

$$P(\Omega^*) \leq P(\Omega) \text{ for all } \Omega \in \mathscr{C},$$

or similarly that Ω^* maximizes P if

$$P(\Omega^*) \geq P(\Omega) \text{ for all } \Omega \in \mathscr{C}.$$

For several reasons, it is useful to limit our discussion to minimization problems. First, each maximization problem is equivalent to minimizing $-P$. Secondly, a majority of the problems encountered in geometric optimization are minimization problems. For example, the study of minimal surfaces, soap films, and dynamical systems all deal in part with minimization problems. For simplicity, we make this restriction.

Now let's turn our attention to optimization problems in geometry. The competitors for a geometric optimization problem may be manifolds that meet some given condition. These could include manifolds with fixed boundary, manifolds that are themselves boundary, or manifolds with fixed mass. Most commonly, this type of optimization problem asks which manifolds minimize length or surface area. In general, we can define the objective function as

$$P(\Omega) = \int_{\Omega} \Phi \text{ for all } \Omega \in S$$

given some general integrand Φ. For mass (length, area, or volume) minimization problems, $\Phi = \text{Vol} = 1$.

2.1 Calibration

In 1982 Harvey and Lawson published their landmark paper, *Calibrated Geometries* [12]. Building on several disparate ideas, they presented a new framework of minimization proof. They found that it is possible to construct an intermediate function that directly proves minimization by using closed differential forms of unit comass. Some key results are summarized below.

2.2 Calibrated Geometries

While calibrated geometries have a natural definition in the realm of arbitrary Riemannian manifolds, in this section we look only at calibrations in $\mathbb{R}^n$. This will suffice to give the reader a taste

of the calibration argument. For the advanced reader, however, more information on calibrations may be found in several texts, such as Frank Morgan's *Geometric Measure Theory: A Beginner's Guide* [20] (c.f. chapter 6 and the reference in section 6.5).

Theorem 2.2.1. ***The Fundamental Theorem of Calibrations.*** *Let φ be a closed differential k-form of unit comass defined on $\mathbb{R}^n$. Suppose that M is a k-dimensional manifold in $\mathbb{R}^n$ such that*

$$\langle \varphi, \xi_M \rangle = 1 \text{ for all } x \in M.$$

Then M is area-minimizing for its boundary.

Proof. The proof of this theorem is famous for its brevity:

Let S be any other k-dimensional manifold in $\mathbb{R}^n$ with the same boundary as M ($\partial S = \partial M$). Then

$$\int_M 1 = \int_M \varphi = \int_S \varphi \leq \int_S 1.$$

□

We call a closed differential form of unit comass a *calibration*. If M is a manifold satisfying the conditions of the previous theorem, then we say that M is *calibrated by* φ.

2.3 Metacalibration

Calibrations have greatly simplified some types of optimization problems, most notably those with fixed boundary. But what happens when we want to use a fixed volume constraint instead?

2.4 An Almost-Proof

Consider the isoperimetric problem of minimizing perimeter while enclosing a given area. Let's see if we can use calibrations to give a proof that the circle has the least perimeter of all figures

with the same area. The main task is finding an appropriate differential form φ that will calibrate the circle.

We can already give some conditions that φ will have to meet. Let Ω^* be the disk of radius r centered at the origin with $\partial\Omega^*$ its bounding circle. In order to calibrate Ω^*, we need to have $\langle\varphi, \xi_{\partial\Omega^*}\rangle = 1$ everwhere on $\partial\Omega^*$. This implies, however, that φ cannot be closed, because $\int_{\partial\Omega^*} 1 = \int_{\partial\Omega^*} \varphi = \int_M d\varphi \neq 0$. We can, however, use still Stokes' theorem in our proof, but in a different way. Let Ω be any other figure in the plane with the same area as Ω^* with $\partial\Omega$ its boundary. Suppose that $d\varphi = c$ for some constant c. Then we see that

$$\begin{aligned} G(\Omega^*) &= \int_{\partial\Omega^*} \varphi \\ &= \int_{\Omega^*} d\varphi \\ &= c\pi r^2 \\ &= \int_{\Omega} d\varphi \\ &= \int_{\partial\Omega} \varphi = G(\Omega). \end{aligned}$$

So we are looking for a differential form φ that is unit on $\partial\Omega^*$ for which $d\varphi$ is constant. This essentially limits us to $\varphi = \frac{-ydx+xdy}{r}$. Let's see if it works.

First, by definition,

$$P(\Omega^*) = \int_{\partial\Omega^*} 1 = \int_{\partial\Omega^*} \langle\varphi, \xi_{\partial\Omega^*}\rangle = G(\Omega^*).$$

Second, since $d\varphi = \frac{2}{r} dx \wedge dy$,

$$G(\Omega^*) = \int_{\Omega^*} \frac{2}{r} dx \wedge dy = \frac{2}{r}\pi r^2 = \int_{\Omega} \frac{2}{r} dx \wedge dy = G(\Omega).$$

Unfortunately, the proof falls apart on the last step. Since $\|\varphi\| > 1$ outside of Ω^*, we run into a statement we can't prove:

$$G(\Omega) = \int_{\partial\Omega} \varphi \leq \int_{\partial\Omega} \|\varphi\| \stackrel{?}{\leq} \int_{\partial\Omega} 1 = P(\Omega).$$

This failure appears unavoidable: when we use any other differential form as our calibration we can always find a competitor that it fails to be unit on. We need to try something else.

2.5 A Proof Indeed

In our attempt to calibrate the circle, the problem we ran into was that no single differential form could handle all the different possible shapes of competitors. If we picked one particular competitor however, it would be relatively easy to find a calibration-type differential form that could handle just that competitor. Why can't we just use those?

Here we find the fundamental concept behind metacalibration: *use a different calibration for each competitor*. Let's see if we can use this idea to construct a proof:

Let $\varphi_{\Omega^*} = \frac{-ydx+xdy}{r}$. For each competitor Ω, we want to create a differential form φ_Ω that acts on Ω like φ_{Ω^*} acts on Ω^*. For each point (x_0, y_0) in Ω, let $a(y_0)$ be the area of S below the line $y = y_0$. Since $\text{Area}(\Omega^*) = \text{Area}(\Omega)$, there exists y^* such that the area of Ω^* below the line $y = y^*$ is equal to $a(y_0)$. Mapping the line segment of $y = y_0$ in Ω linearly onto the line segment of $y = y^*$ in Ω^* lets us also define x^* as the image of x_0 under this map. This mapping is shown visually below. Let $\varphi_\Omega(x_0, y_0) = \frac{-y^*(y_0)dx+x^*(x_0,y_0)dy}{r}$ and $G(\Omega) = \int_\Omega \varphi_\Omega$.

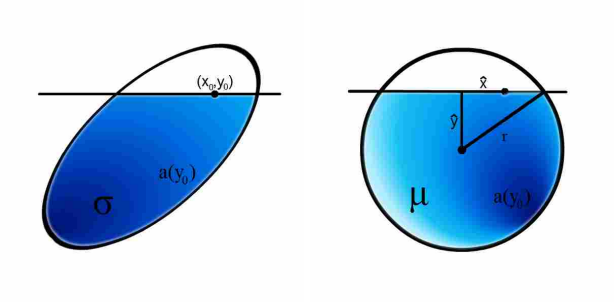

Figure 2.1 Slicing Methods

Since the map $(x, y) \mapsto (x^*, y^*)$ is area preserving, we find that $\frac{\partial x^*}{\partial x}\frac{\partial y^*}{\partial y} = 1$ and, by the algebraic

mean-geometric mean inequality, $2 \leq \frac{\partial x^*}{\partial x} + \frac{\partial y^*}{\partial y}$. Thus,

$$\begin{aligned} G(\Omega^*) &= \int_{\partial\Omega^*} \varphi_{\Omega^*} \\ &= \int_{\Omega^*} d\varphi_{\Omega^*} = \int_{\Omega^*} \frac{2}{r} \\ &= \frac{2}{r}\pi r^2 \\ &= \int_{\Omega} \frac{2}{r} \\ &\leq \int_{\Omega} \frac{\frac{\partial x^*}{\partial x} + \frac{\partial y^*}{\partial y}}{r} = \int_{\Omega} d\varphi_{\Omega} \\ &= \int_{\partial\Omega} \varphi_{\Omega} = G(\Omega) \end{aligned}$$

But since $\|\varphi_{\Omega}\| \leq 1$ everywhere on Ω, we also have

$$G(\Omega) = \int_{\partial\Omega} \varphi_{\Omega} \leq \int_{\partial\Omega} \|\varphi_{\Omega}\| \leq \int_{\partial\Omega} 1 ds = P(\Omega).$$

Putting these results together we get

$$P(\Omega^*) = G(\Omega^*) \leq G(\Omega) \leq P(\Omega)$$

and we have a proof indeed.

2.6 The Metacalibration Theorem

Based on the previous section, we can see that that key difference between calibration and metacalibration methods is that *calibrations use a single differential form for all competitors, while metacalibrations use a unique differential form for each competitor.* We formalize this difference in the following definition.

Definition 2.6.1. Given a set of competitors $\mathscr{C}$, a *metacalibration* is a set of differential forms $\{\varphi_{\Omega} \in \mathscr{A}^k(\Omega) | \text{ for all } \Omega \in \mathscr{C}\}$ such that for all $\Omega \in \mathscr{C}$ and for some $\Omega^* \in \mathscr{C}$,

MC I. $\langle \varphi_\Omega(x), \xi_\Omega(x) \rangle \leq 1$ for all $x \in \Omega$,

MC II. $\langle \varphi_{\Omega^*}(x), \xi_{\Omega^*}(x) \rangle = 1$ for all $x \in \Omega^*$, and

MC III. $\int_{\Omega^*} \varphi_{\Omega^*} \leq \int_\Omega \varphi_\Omega$.

In this sense we say that the metacalibration, $\{\varphi_\Omega\}$, *calibrates* Ω^*.

Theorem 2.6.2. ***Metacalibration Theorem.*** *Let $\mathscr{C}$ be a set of competitors, and suppose that $\{\varphi_\Omega\}$ is a metacalibration for $\mathscr{C}$ that calibrates $\Omega^* \in \mathscr{C}$. Then Ω^* is mass-minimizing in $\mathscr{C}$.*

Proof. Let $G(\Omega) = \int_\Omega \varphi_\Omega$ for all $\Omega \in \mathscr{C}$. Then

$$\begin{aligned} P(\Omega^*) &= \int_{\Omega^*} 1 \\ &= \int_{\Omega^*} \langle \varphi_{\Omega^*}, \xi_{\Omega^*} \rangle \\ &= G(\Omega^*) \leq G(\Omega) \\ &= \int_\Omega \langle \varphi_\Omega, \xi_\Omega \rangle \\ &\leq \int_\Omega 1 = P(\Omega). \end{aligned}$$

□

At this point the major parts of a metacalibration proof become apparent. First, you need to identify what competitor you believe is the minimizer. Second, you need to develop the metacalibration with that conjectured minimizer as a basis. Typically, the first problem is easy to solve: good guesses, computer simulations, and observing nature can all help. The second problem proves much more difficult. We usually construct metacalibrations using the process of emulation to model the differential form on a competitor Ω after a natural differential form on Ω^*.

Part II

Proof of the Double Bubble Conjecture in $\mathbb{R}^n$

Chapter 3

A New Proof of the Double Bubble Conjecture in $\mathbb{R}^n$ and an Extension to Surfaces with Boundary: By James Dilts, Rebecca Dorff, and Donald Sampson

3.1 Introduction

In this paper we give a new proof of the double bubble conjecture: that the least surface area way to separately enclose two given volumes in $\mathbb{R}^n$ is the so called ï£¡standard double bubbleï£¡ composed of three spherical caps meeting at 120°. This conjecture was first proven by Hutchings, Morgan, Ritoré, and Ros [13] using the calculus of variations. Our proof uses instead a calibration type argument similar to the Knothe-Gromov proof of the Isoperimetric inequality.

The relatively new method of calibration, first popularized by Harvey and Lawson [12], has been used in a variety of circumstances to solve surface area minimization problems. Typical

problems include mass-minimization given a fixed boundary condition.

Our method is a generalization of this approach that can incorporate a fixed volume condition. We call our method *metacalibration*. In particular it is a direct style of proof in which characteristics of the conjectured minimizer are used to construct the necessary inequalities.

Let Ω be any admissible competitor, and let Ω^* be the conjectured minimizer. Given an objctive functional P, calibration proofs typically take the form

$$P(\Omega^*) = G(\Omega^*) \leq G(\Omega) \leq P(\Omega),$$

where G is an intermediary function defined using the characteristics of both Ω and Ω^*. In what follows we let $G(\Omega) = \int_{\partial\Omega} \langle \varphi_\Omega, \vec{n} \rangle dA$ for φ_Ω defined separately on each competitor. This approach unifies several proofs into a common frame work, such as those of Knothe-Gromov [11], Schmidt [21], Lawlor [17], Dilts [5], and Brenier-McCann [19].

In this paper we use this approach to generalize the Knothe-Gromov proof of the isoperimetric inequality to two enclosed areas. In Section 3.2 we review the Knothe-Gromov approach and the proof of the standard isoperimetric inequality using this method. Section 3.3 presents our generalization of the Knothe rearrangement to two volumes and defines the intermediate function G for all competitors. We finish the proof in Section 3.4 by proving the three inequalities mentioned above. Section 3.5 demonstrates how these results extend to solutions of the equitent problem [8] of double bubbles with boundary constraint.

3.2 The Knothe-Gromov Proof of the Isoperimetric Inequality in $\mathbb{R}^n$

The following proof is due to Mikhail Gromov [11]. It relies primarily on a map from any competitor Ω to the minimizing ball Ω^* constructed by mapping 'slices' of one to 'slices' of the other. This

map is now known as the Knothe-Rosenblatt rearrangement, developed independently by Herbert Knothe [16] and Murry Rosenblatt [22]. We construct this map as follows:

Let Ω be any competitor (open domain) of fixed volume, and let Ω^* be the ball of the same volume centered at the origin. Let r be the radius of Ω^*. We define $F : \Omega \to \Omega^*$ by $(y_1, y_2, \ldots, y_n) \mapsto (z_1, z_2, \ldots, z_n)$ such that

$$\begin{aligned}&\frac{\mathrm{Vol}(\Omega \cap \{x_1 = y_1, \ldots, x_{j-1} = y_{j-1}, x_j \leq y_j\})}{\mathrm{Vol}(\Omega \cap \{x_1 = y_1, \ldots, x_{j-1} = y_{j-1}\})}\\ =&\frac{\mathrm{Vol}(\Omega^* \cap \{x_1 = z_1, \ldots, x_{j-1} = z_{j-1}, x_j \leq z_j\})}{\mathrm{Vol}(\Omega^* \cap \{x_1 = z_1, \ldots, x_{j-1} = z_{j-1}\})}\end{aligned}$$

for all $1 \leq j \leq n$. Scaled volume is preserved set-wise under each 'slice,' with the last coordinate mapped (locally) linearly on the final 'slice' of a portion of a line in Ω mapped to a line segment in Ω^*. Volume is then preserved pointwise, so that $\det DF = 1$. Note that F_j is seen to depend only on the variables $\{x_1, x_2, \ldots, x_j\}$, so that DF is lower triangular with positive diagonal entries. Lastly, if $\Omega = \Omega^*$ then F is simply the identity on Ω^*. The details of this construction of were worked out by Brothers and Morgan in [3]. They also provide a version of the divergence theorem with weakened hypotheses and show that F satisfies these.

We now give the proof after Gromov:

Theorem 3.2.1. *The $n-1$-sphere is the least surface area figure in $\mathbb{R}^n$ among all those that enclose a fixed volume.*

Proof. Given any competitor Ω, let $P(\Omega)$ be the surface area of Ω. Let $\varphi_\Omega = \frac{F(x_1, x_2, \ldots x_n)}{r}$, and let $G(\Omega) = \int_{\partial\Omega} \langle \varphi_\Omega, \vec{n} \rangle dA$ where $\vec{n}$ is the unit normal to the figure. This yields

$$\begin{aligned}G(\Omega) &= \int_{\partial\Omega} \langle \varphi_\Omega, \vec{n} \rangle dA\\ &\leq \int_{\partial\Omega} \|\varphi_\Omega\| dA\\ &\leq \int_{\partial\Omega} dA\\ &= P(\Omega).\end{aligned}$$

since φ_Ω is at most a unit vector. Note also that if $\Omega = \Omega^*$, we have equality ($P(\Omega^*) = G(\Omega^*)$) since $\varphi_{\Omega^*} = \vec{n}$ on $\partial\Omega^*$.

Now consider that $\operatorname{div}\varphi_\Omega = \frac{1}{r}\operatorname{div} F = \frac{1}{r}\operatorname{tr} DF$. Since $\prod_{i=1}^n \frac{\partial F_i}{\partial x_i} = \det DF = 1$, the arithmetic mean-geometric mean inequality implies that $n \leq \operatorname{tr} DF$. Thus $\frac{n}{r} \leq \operatorname{div}\varphi_\Omega$. Therefore

$$\begin{aligned}
G(\Omega^*) &= \int_{\partial\Omega^*} \langle \varphi_{\Omega^*}, \vec{n}\rangle dA \\
&= \int_{\Omega^*} \operatorname{div}\varphi_{\Omega^*} dV \\
&= \int_{\Omega^*} \frac{n}{r} dV \\
&= \frac{n\operatorname{Vol}(\Omega^*)}{r} \\
&= \int_{\Omega} \frac{n}{r} dV \\
&\leq \int_{\Omega} \operatorname{div}\varphi_\Omega dV \\
&= \int_{\partial\Omega} \langle \varphi_\Omega, \vec{n}\rangle dA \\
&= G(\Omega).
\end{aligned}$$

Putting these three results together gives the famous one line proof common to all calibration arguments:

$$P(\Omega^*) = G(\Omega^*) \leq G(\Omega) \leq P(\Omega).$$

□

3.3 Generalization to Two Volumes

In this section we describe a variation on the Knothe-Rosenblatt rearrangement for two volumes. The key idea is to 'tilt' the slices to match volume in both bubbles. This map fails to preserve volume locally, but we show in the following section that the necessary inequalities still hold when averaged over slices. We then complete the proof of the double bubble conjecture in that section.

Let Ω be an arbitrary competitor double bubble in $\mathbb{R}^n$. Thus $\Omega = \Omega_1 \cup \Omega_2$ where the Ω_i are disjoint open domains of fixed volume that may or may not share boundary. It was shown by Foisy et al. in [10] that there exists a standard double bubble in $\mathbb{R}^n$ that separately encloses volumes $\mathrm{Vol}(\Omega_1)$ and $\mathrm{Vol}(\Omega_2)$. Denote the standard double bubble as $\Omega^* = \Omega_1^* \cup \Omega_2^*$ where $\mathrm{Vol}(\Omega_i) = \mathrm{Vol}(\Omega_i^*)$. Now each Ω_i has a natural center o_i as the center of the spherical cap that forms its exterior face. Similarly the interface between Ω_1 and Ω_2 is a spherical cap with center o_3. Denote the radii of these three spherical caps r_i respectively. In all standard double bubbles $\frac{1}{r_3} = \frac{1}{r_1} - \frac{1}{r_2}$ [14]. Note that the o_i are also collinear. Orient Ω^* so that o_1 is the origin and o_2 lies on the positive x_1 axis.

Given a slice of Ω, our goal is to find a corresponding slice in Ω^* that has the same area under the slice in each corresponding bubble. Unfortunately, this is not always possible. In particular, if the enclosed areas are not equal there is no hyper-plane through Ω^* that separates them. We get around this by reorienting our competitor Ω. By the so-called ham-sandwich theorem, there is a hyper-plane that splits both volumes exactly in half. If we slice Ω parallel to this hyper-plane, every slice of Ω will have a corresponding slice in Ω^*. Without loss of generality, we assume that these hyper-planes are oriented with the coordinate hyper-planes appropriately. This means that while the slices in Ω are all parallel, the slices in Ω^* will tilt and may intersect. This represents the image space, Ω^*, in a rotating frame of reference. Further details of this mapping were worked out in [9], so we assume we are able to define the mappings $F_i : \Omega_i \to \Omega^*$ as follows:

Given $\vec{z} = (z_1, z_2, \ldots, z_n) \in \Omega_i$, denote the slice of Ω^* corresponding (as above) to the hyper-plane $\{x_n = z_n\}$ by S_n. Let y_i^n be the signed distance from o_i to S_n. (We let $y_i^n > 0$ if S_n is above o_i, and $y_i^n < 0$ otherwise.) As in the single bubble case, we now consider 'slices of slices'. The slice S_n is itself a (weighted) double bubble in one less dimension. Let S_{n-1} be the slice of $\Omega^* \cap S_n$ that corresponds to the hyper-plane $\{x_{n-1} = z_{n-1}\}$ in $\Omega \cap \{x_n = z_n\}$. Let y_i^{n-1} be the signed distance from the projection of o_i on S_n to the slice S_{n-1}. Proceed in the same fashion to define $y_i^{n-1}, \ldots, y_i^1$

and let $F_i(\vec{z}) = (y_i^1, y_i^2, \ldots, y_i^n)$.

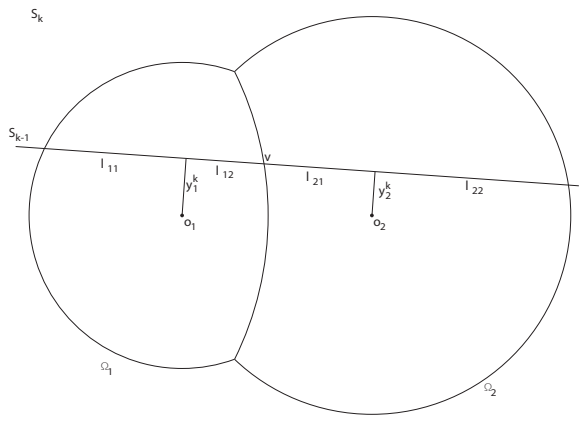

Figure 3.1 Tilted Slicing

When we take slices of slices, there is no guarantee that the total volume of a slice in Ω to match that of its corresponding slice in Ω^*. Instead of matching volume under the slice, we match the volume fraction, or scaled volume. Denote $\mathrm{Vol}(\Omega_i \cap \{x_n = z_n, \ldots, x_k = z_{k+1}\})$ as V_i^k and $\mathrm{Vol}(\Omega_i^* \cap S_{k+1})$ as V_i^{k*}. By convention we let $V_i^{n(*)} = \mathrm{Vol}^n(\Omega_i^{(*)})$.

3.4 Proof of the Double Bubble Conjecture

We now use the map defined in the previous section to construct a metacalibration. We then show that the intermediary function thus defined satisfies the three inequalities, $P(\Omega^*) = G(\Omega^*) \leq G(\Omega) \leq P(\Omega)$.

The maps $F_i : \Omega_i \to \Omega_i^*$ can also be considered as a vector field on Ω_i. We scale these to define two new vector fields. Let

$$\varphi_{\Omega_i}(\vec{z}) = \frac{F_i(\vec{z})}{r_i}.$$

We define our intermediary function as

$$G(\Omega) = \int_{\partial\Omega_1} \langle \varphi_{\Omega_1}, \vec{n} \rangle d\,\mathrm{Vol}^{n-1} + \int_{\partial\Omega_2} \langle \varphi_{\Omega_2}, \vec{n} \rangle d\,\mathrm{Vol}^{n-1},$$

where $\vec{n}$ is the unit exterior normal to the boundary surfaces. We now separately prove each of the above inequalities.

Lemma 3.4.1. $P(\Omega^*) = G(\Omega^*)$

Proof. First note that for any point on the exterior boundary of Ω_i^* the vector $\varphi_{\Omega_i^*}$ is equal to the unit normal. Thus $\langle \varphi_{\Omega_i^*}, \vec{n} \rangle = 1$. It was also shown in [9] that at all points on the interior boundary $\partial\Omega_1^* \cap \partial\Omega_2^*$, $\langle \varphi_{\Omega_1^*} - \varphi_{\Omega_2^*}, \vec{n} \rangle = 1$. Thus by definition of $G(\mu)$,

$$\begin{aligned} G(\Omega^*) &= \int_{\partial\Omega_1^* - \partial\Omega_2^*} \langle \varphi_{\Omega_1^*}, \vec{n} \rangle d\,\mathrm{Vol}^{n-1} + \int_{\partial\Omega_2^* - \partial\Omega_1^*} \langle \varphi_{\Omega_2^*}, \vec{n} \rangle d\,\mathrm{Vol}^{n-1} \\ &\quad + \int_{\partial\Omega_1^* \cap \partial\Omega_2^*} \langle \varphi_{\Omega_1^*} - \varphi_{\Omega_2^*}, \vec{n} \rangle d\,\mathrm{Vol}^{n-1} \\ &= \int_{\partial\Omega_1^* - \partial\Omega_2^*} d\,\mathrm{Vol}^{n-1} + \int_{\partial\Omega_2^* - \partial\Omega_1^*} d\,\mathrm{Vol}^{n-1} + \int_{\partial\Omega_1^* \cap \partial\Omega_2^*} d\,\mathrm{Vol}^{n-1} \\ &= \int_{\partial\Omega_1^* \cup \partial\Omega_2^*} d\,\mathrm{Vol}^{n-1} = P(\Omega^*). \end{aligned}$$

□

Lemma 3.4.2. $G(\Omega) \leq P(\Omega)$

Proof. Since $F_i(\vec{z})$ always lies on or inside a sphere of radius r_i, $||\varphi_{\Omega_i}|| \leq 1$. It was also shown in [9] that on the shared boundary of the two bubbles, $\langle \varphi_{\Omega_1^*} - \varphi_{\Omega_2^*}, \vec{n} \rangle \leq 1$. Thus we find that

$$\begin{aligned} G(\Omega) &= \int_{\partial\Omega_1} \langle \varphi_{\Omega_1}, \vec{n} \rangle d\,\mathrm{Vol}^{n-1} + \int_{\partial\Omega_2} \langle \varphi_{\Omega_2}, \vec{n} \rangle d\,\mathrm{Vol}^{n-1} \\ &= \int_{\partial\Omega_1 - \partial\Omega_2} \langle \varphi_{\Omega_1}, \vec{n} \rangle d\,\mathrm{Vol}^{n-1} + \int_{\partial\Omega_2 - \partial\Omega_1} \langle \varphi_{\Omega_2}, \vec{n} \rangle d\,\mathrm{Vol}^{n-1} \\ &\quad + \int_{\partial\Omega_1 \cap \partial\Omega_2} \langle \varphi_{\Omega_1} - \varphi_{\Omega_2}, \vec{n} \rangle d\,\mathrm{Vol}^{n-1} \\ &\leq \int_{\partial\Omega_1 - \partial\Omega_2} \|\varphi_{\Omega_1}\| d\,\mathrm{Vol}^{n-1} + \int_{\partial\Omega_2 - \partial\Omega_1} \|\varphi_{\Omega_2}\| d\,\mathrm{Vol}^{n-1} + \int_{\partial\Omega_1 \cap \partial\Omega_2} d\,\mathrm{Vol}^{n-1} \\ &\leq \int_{\partial\Omega_1 - \partial\Omega_2} d\,\mathrm{Vol}^{n-1} + \int_{\partial\Omega_2 - \partial\Omega_1} d\,\mathrm{Vol}^{n-1} + \int_{\partial\Omega_1 \cap \partial\Omega_2} d\,\mathrm{Vol}^{n-1} \\ &= \int_{\partial\Omega_1 \cup \partial\Omega_2} d\,\mathrm{Vol}^{n-1} = P(\Omega). \end{aligned}$$

□

This last lemma is the crux of the proof. We prove that the necessary inequalities hold when integrated over slices.

Lemma 3.4.3. $G(\Omega^*) \leq G(\Omega)$

Proof. As an application of the divergence theorem, we have

$$\begin{aligned} G(\Omega^*) &= \int_{\partial\Omega_1^*} \langle \varphi_{\Omega_1^*}, \vec{n} \rangle d\,\mathrm{Vol}^{n-1} + \int_{\partial\Omega_2^*} \langle \varphi_{\Omega_2^*}, \vec{n} \rangle d\,\mathrm{Vol}^{n-1} \\ &= \int_{\Omega_1^*} \operatorname{div} \varphi_{\Omega_1^*} d\,\mathrm{Vol}^n + \int_{\Omega_2^*} \operatorname{div} \varphi_{\Omega_2^*} d\,\mathrm{Vol}^n \\ &= \int_{\Omega_1^*} \frac{n}{r_1} d\,\mathrm{Vol}^n + \int_{\Omega_2^*} \frac{n}{r_2} d\,\mathrm{Vol}^n \\ &= \frac{n\,\mathrm{Vol}^n(\Omega_1^*)}{r_1} + \frac{n\,\mathrm{Vol}^n(\Omega_2^*)}{r_2} \\ &= \frac{n\,\mathrm{Vol}^n(\Omega_1)}{r_1} + \frac{n\,\mathrm{Vol}^n(\Omega_2)}{r_2}. \end{aligned}$$

Letting F_i^j be the jth coordinate of F_i, we also have

$$\begin{aligned} G(\Omega) &= \int_{\partial\Omega_1} \langle \varphi_{\Omega_1}, \vec{n} \rangle d\,\mathrm{Vol}^{n-1} + \int_{\partial\Omega_2} \langle \varphi_{\Omega_2}, \vec{n} \rangle d\,\mathrm{Vol}^{n-1} \\ &= \int_{\Omega_1} \operatorname{div} \varphi_{\Omega_1} d\,\mathrm{Vol}^n + \int_{\Omega_2} \operatorname{div} \varphi_{\Omega_2} d\,\mathrm{Vol}^n \\ &= \int_{\Omega_1} \frac{\sum_{j=1}^n \frac{\partial F_1^j}{\partial x_j}}{r_1} d\,\mathrm{Vol}^n + \int_{\Omega_2} \frac{\sum_{j=1}^n \frac{\partial F_2^j}{\partial x_j}}{r_2} d\,\mathrm{Vol}^n. \end{aligned}$$

To finish the argument we first prove a set of propositions. In the following we use the notation given in Figure 3.2. Given a slice S_k of Ω^*, an infinitesimal change dx_k will cause a tilt in S_k, causing an angle $d\theta$ to form.

Proposition 3.4.4.

$$\frac{l_{11}^2 - l_{12}^2}{r_1} = \frac{l_{22}^2 - l_{21}^2}{r_2}.$$

Proof. Note that $l_{11}^2 - l_{12}^2 = (l_{11} + l_{12})(l_{11} - l_{12})$, which is the product of the two lengths of a chord though the point v. This product is constant over all chords through v, and in particular

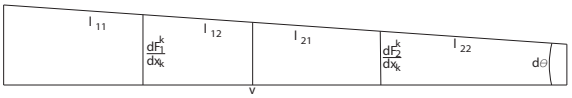

Figure 3.2 An Infinitesimal Change

for a diameter. Thus $l_{11}^2 - l_{12}^2 = (l_{11}+l_{12})(l_{11}-l_{12}) = (r_1+s_1)(r_1-s_1) = r_1^2 - s_1^2$ and similarly $l_{21}^2 - l_{22}^2 = r_2^2 - s_2^2$. It was shown in [9] that $\frac{r_1^2-s_1^2}{r_1} = \frac{r_2^2-s_2^2}{r_2}$. This completes the proof. □

Proposition 3.4.5.

$$\frac{1}{r_1}\left(V_1^{k-1}\frac{V_1^{k*}}{V_1^k} - V_1^{k-1*}\frac{\partial F_1^k}{\partial x_k}\right) = -\frac{1}{r_2}\left(V_2^{k-1}\frac{V_2^{k*}}{V_2^k} - V_2^{k-1*}\frac{\partial F_2^k}{\partial x_k}\right) = \lambda_k$$

Proof. Let $W_i^{k(*)}$ be the volume underneath the 'slice' in $\Omega^{(*)}$. Consider then that according to our weighting of slices

$$V_i^{k-1}\frac{V_i^{k*}}{V_i^k} = \frac{\partial W_i^k}{\partial x_k}\frac{V_i^{k*}}{V_i^k} = \frac{\partial W_i^{k*}}{\partial x_k}.$$

Now the value $\frac{\partial W_i^{k*}}{\partial x_k}$ represents the change in volume under the slice in Ω^*, or equivalently the volume between two infinitesimally near slices of Ω^*. Suppose as in figure 3.2 that the infinitesimal change in tilt of the slices is to the right. Then

$$\begin{aligned}\frac{\partial W_i^{k*}}{\partial x_k} &= \int_{S_{k-1}} V_i^{1*}\frac{\partial F_i^k}{\partial x_k} + \frac{l_{i1}^2 - l_{i2}^2}{2}\frac{d\theta}{dx_k}dx_2\cdots dx_{k-1} \\ &= V_i^{k-1*}\frac{\partial F_1^k}{\partial x_k} + \int_{S_{k-1}} \frac{l_{i1}^2 - l_{i2}^2}{2}\frac{d\theta}{dx_k}dx_2\cdots dx_{k-1}.\end{aligned}$$

But by the previous proposition

$$\begin{aligned}\frac{1}{r_1}\left(\frac{\partial W_1^{k*}}{\partial x_k} - V_1^{k-1*}\frac{\partial F_1^k}{\partial x_k}\right) &= \int_{S_{k-1}} \frac{l_{11}^2 - l_{12}^2}{2r_1}\frac{d\theta}{dx_k}dx_2\cdots dx_{k-1} \\ &= -\int_{S_{k-1}} \frac{l_{21}^2 - l_{22}^2}{2r_2}\frac{d\theta}{dx_k}dx_2\cdots dx_{k-1} \\ &= -\frac{1}{r_2}\left(\frac{\partial W_2^{k*}}{\partial x_k} - V_2^{k-1*}\frac{\partial F_2^k}{\partial x_k}\right).\end{aligned}$$

The same result holds with signs reversed ($\lambda_k < 0$) for a tilt to the left. Substitution finishes the proof. □

Proposition 3.4.6.

$$\sum_{i=1,2} \frac{\left((k-1)\left(\frac{V_i^{k-1*}}{V_i^{k-1}}\right)^{1/(k-1)} + \frac{\partial F_i^k}{\partial x_k}\right)V_i^{k-1}}{r_i} \geq \sum_{i=1,2} \frac{k\left(\frac{V_i^{k*}}{V_i^k}\right)^{1/k} V_i^{k-1}}{r_i}.$$

Proof. Starting out with the generalized arithmetic mean-geometric mean inequality we have:

$$\begin{aligned}&\sum_{i=1,2} \frac{\left((k-1)\left(\frac{V_i^{k-1*}}{V_i^{k-1}}\right)^{1/(k-1)} + \frac{\partial F_i^k}{\partial x_k}\right)V_i^{k-1}}{r_i} \\ &\quad\geq \sum_{i=1,2} \frac{k\left(\frac{V_i^{k-1*}}{V_i^{k-1}}\frac{\partial F_i^k}{\partial x_k}\right)^{1/k} V_i^{k-1}}{r_i} \\ &\quad= \sum_{i=1,2} \frac{k\left(\frac{V_i^{k-1*}}{V_i^{k-1}}\left(\frac{V_i^{k-1}}{V_i^{k-1*}}\frac{V_i^{k*}}{V_i^k} + (-1)^i\frac{r_i}{V_i^{k-1*}}\lambda_k\right)\right)^{1/k} V_i^{k-1}}{r_i} \\ &\quad= \sum_{i=1,2} \frac{k\left(\frac{V_i^{k*}}{V_i^k} + (-1)^i\frac{r_i}{V_i^{k-1}}\lambda_k\right)^{1/k} V_i^{k-1}}{r_i} = H_k\end{aligned}$$

We now optimize this expression in terms of λ_k. Now

$$\frac{\partial H_k}{\partial \lambda_k} = \sum_{i=1,2}(-1)^i\left(\frac{V_i^{k*}}{V_i^k} + (-1)^i\frac{r_i}{V_i^{k-1}}\lambda_k\right)^{(1-k)/k} = 0$$

if and only if $\frac{V_1^{k-1*}}{V_1^{k-1}}\frac{\partial F_1^k}{\partial x_k} = \frac{V_2^{k-1*}}{V_2^{k-1}}\frac{\partial F_2^k}{\partial x_k}$. This only occurs when $\lambda_k = 0$ (in the absence of any change in tilt), which gives a minimum value of H_k. Thus

$$H_k \geq \sum_{i=1,2} \frac{k\left(\frac{V_i^{k*}}{V_i^k}\right)^{1/k} V_i^{k-1}}{r_i},$$

completing the proof. □

From Proposition 3.4.6 we have the following inequalities by integrating over each slice in turn.

$$\begin{aligned}
&\sum_{i=1,2}\int_{\Omega_i} \frac{\frac{\partial F_i^k}{\partial x_k} + (k-1)\left(\frac{V_i^{k-1*}}{V_i^{k-1}}\right)^{1/(k-1)}}{r_i} dx_1\cdots dx_n \\
&= \sum_{i=1,2}\int_{\Omega_i} \frac{\left(\frac{\partial F_i^k}{\partial x_k} + (k-1)\left(\frac{V_i^{k-1*}}{V_i^{k-1}}\right)^{1/(k-1)}\right) V_i^{k-1}}{r_i} dx_k\cdots dx_n \\
&\geq \sum_{i=1,2}\int_{\Omega_i} \frac{k\left(\frac{V_i^{k*}}{V_i^k}\right)^{1/k} V_i^{k-1}}{r_i} dx_k\cdots dx_n \\
&\geq \sum_{i=1,2}\int_{\Omega_i} \frac{k\left(\frac{V_i^{k*}}{V_i^k}\right)^{1/k}}{r_i} dx_1\cdots dx_n
\end{aligned}$$

Since $\frac{\partial F_i^1}{\partial x_1} = \frac{V_i^{1*}}{V_i^1}$, this gives the following chain of inequalities.

$$\begin{aligned}
\sum_{i=1,2}\int_{\Omega_i}\frac{\sum_{k=1}^{n}\frac{\partial F_i^k}{\partial x_k}}{r_i}d\,\mathrm{Vol}^n &= \sum_{i=1,2}\int_{\Omega_i}\frac{\sum_{k=2}^{n}\frac{\partial F_i^k}{\partial x_k}+\frac{V_i^{1*}}{V_i^1}}{r_i}dx_1\cdots dx_n\\
&\geq \sum_{i=1,2}\int_{\Omega_i}\frac{\sum_{k=3}^{n}\frac{\partial F_i^k}{\partial x_k}+2\left(\frac{V_i^{2*}}{V_i^2}\right)^{1/2}}{r_i}dx_1\cdots dx_n\\
&\geq \cdots\\
&\geq \sum_{i=1,2}\int_{\Omega_i}\frac{\frac{\partial F_i^n}{\partial x_n}+(n-1)\left(\frac{V_i^{n-1*}}{V_i^{n-1}}\right)^{1/(n-1)}}{r_i}dx_1\cdots dx_n\\
&\geq \sum_{i=1,2}\int_{\Omega_i}\frac{n\left(\frac{V_i^{n*}}{V_i^n}\right)^{1/n}}{r_i}dx_1\cdots dx_n\\
&= \sum_{i=1,2}\int_{\Omega_i}\frac{n\left(\frac{\mathrm{Vol}^n(\Omega_i^*)}{\mathrm{Vol}^n(\Omega_i)}\right)^{1/n}}{r_i}dx_1\cdots dx_n\\
&= \sum_{i=1,2}\int_{\Omega_i}\frac{n}{r_i}dx_1\cdots dx_n\\
&= \frac{n\,\mathrm{Vol}^n(\Omega_1)}{r_1}+\frac{n\,\mathrm{Vol}^n(\Omega_2)}{r_2}
\end{aligned}$$

Combining this with our earlier evaluations gives us $G(\Omega^*)\leq G(\Omega)$ and completes the proof.

□

Theorem 3.4.7. *The standard double bubble is the least mass hyper-surface in $\mathbb{R}^n$ among all those that separately contain two given n-volumes.*

Proof. By lemmas 3.4.1, 3.4.2, and 3.4.3,

$$P(\mu)=G(\mu)\leq G(\sigma)\leq P(\sigma).$$

This completes the proof. □

3.5 Double Bubble Equitent Problems

The double bubble conjecture has been proven previously using calculus of variations (see [13]). The key to this proof was the use of rotational symmetry. Unfortunately, when boundary constraints are included there is no such symmetries. Consider for example the surface in Figure 3.3. Following [8] however, our metacalibration approach can be combined with external vector fields (using paired calibration a la Lawlor and Morgan, [18]) to prove minimization. For example, it is easy to show that the surface in Figure 3.3 is area minimizing among surfaces that contain the same volumes and span the same boundary.

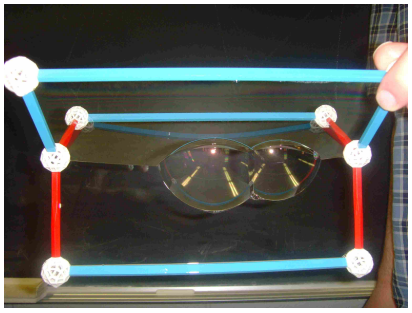

Figure 3.3 An Equitent Surface with Two Volumes

3.6 Conclusion

Using the techniques of metacalibration, we have reproved the double bubble conjecture and extended this result to so-called 'equitent' surfaces with boundary. To do this we adapted the Knothe-Rosenblatt rearrangement to a simultaneous mapping of two volumes. Unfortunately, the natural generalization to three volumes is not generally possible due to the failure of the 'ham-sandwich' theorem for three areas in two dimensions. We do believe however that this approach can be used to reduce the triple bubble conjecture in three or more dimensions to a statement about weighted triple bubbles in the plane.

Seeing that metacalibration unifies many different approaches, it is natural to ask whether another method besides the Knothe-Rosenblatt rearrangement can be used to create a metacalibration function for multiple bubble problems? The most promising alternate method is that of optimal transport. McCann [19] showed that the Brenier map, found as the solution to an optimal mass transport problem, can be used as a metacalibration function in proving the isoperimetric inequality. We hope that a variation of this map may be made to handle multiple bubbles. Such an approach could conceivably prove the $n+1$-bubble conjecture in $\mathbb{R}^n$, including the as yet unproven triple and quadruple bubble conjectures in $\mathbb{R}^3$.

Part III

Equitent Problems

Chapter 4

Isoperimetric Surfaces with Boundary: By Rebecca Dorff, Drew Johnson, Gary Lawlor, and Donald Sampson

We prove that many common combinations of soap films and soap bubbles that result from dipping polyhedral wire frames in soap solution are minimizing with respect to their boundary and bubble volume. This can be thought of as a combination of the Plateau problem of least area for surfaces spanning a given boundary and the isoperimetric problem of least area for surfaces enclosing a given volume. Proof is given in arbitrary dimension using a combination of the mapping of Gromov [11] after Knothe [16] and the paired calibrations of Lawlor and Morgan [18].

4.1 Introduction

In this paper, we prove that many common soap-film-like surfaces that enclose a volume and have a regular polytope "wireframe" as boundary are mass minimizing with respect to their boundary and enclosed volume. Examples of such surfaces are shown in Figure 4.1. We give a direct proof

using the flux of specialized vector fields to model the mass of each competitor a la Gromov [11] and Lawlor and Morgan [18].

We propose the name of "equitent problem" for an area minimization question in which competitors must enclose a given volume ("equal content") as well as span a given boundary ("equal extent"). Equitent problems are thus a generalization of Plateau problems (fixed boundary) and isoperimetric problems (fixed enclosed volume). The equitent problem appears largely unexplored to date; we give what we believe to be the first major results.

4.2 Knothe-Gromov

In 1989 Mikhail Gromov [11], following work of Herbert Knothe, described a beautiful method for proving isoperimetric theorems. He used what is now called the Knothe-Rosenblatt rearrangement, developed independently by Knothe [16] and Rosenblatt [22], which we now describe. Construct an area-preserving map F from a competitor U to the round ball B of radius r (centered at the origin) of the same volume by sending 'slices' of U to 'slices' of B, and repeating the same process in each slice. Specifically, let this map be given by

$$F : U \to B$$

$$(y_1, y_2, \ldots, y_n) \mapsto (z_1, z_2, \ldots, z_n)$$

such that

$$\frac{\mathscr{H}^{n-j+1}U \cap \{x_1 = y_1, \ldots, x_{j-1} = y_{j-1}, x_j \leq y_j\}}{\mathscr{H}^{n-j+1}U \cap \{x_1 = y_1, \ldots, x_{j-1} = y_{j-1}\}} = \frac{\mathscr{H}^{n-j+1}B \cap \{x_1 = z_1, \ldots, x_{j-1} = z_{j-1}, x_j \leq z_j\}}{\mathscr{H}^{n-j+1}B \cap \{x_1 = z_1, \ldots, x_{j-1} = z_{j-1}\}}$$

for all $1 \leq j \leq n$. Thus F_j is seen to depend only on the variables $\{x_1, x_2, \ldots, x_j\}$. Scaled volume is preserved set-wise under each 'slice,' with the last coordinate mapped (locally) linearly on the final 'slice' of a portion of a line in U mapped to a line segment in B. Volume is then preserved pointwise. In addition, if $U = B$ then F is simply the identity on B.

This scheme makes DF lower triangular with positive diagonal entries. Since $\prod_{i=1}^{n} \frac{\partial F_i}{\partial x_i} = \det DF = 1$, the arithmetic-geometric mean inequality implies that $\operatorname{tr} DF \geq n$. Thinking of F as a vector field on U, $\operatorname{tr} DF = \operatorname{div} F \geq n$. Now since the image of F is a ball of radius r, the length of the vector $\frac{1}{r}F(\mathbf{x})$ is always at most 1. The divergence theorem then gives us that

$$\mathscr{H}^{n-1}\partial U = \int_{\partial U} 1 \geq \int_{\partial U} \frac{1}{r} F \cdot \mathbf{n} = \int_U \frac{1}{r} \operatorname{div} F \geq \frac{n}{r} \cdot \mathscr{H}^n U,$$

with equality for the ball. The standard isoperimetric inequality in $\mathbb{R}^n$ results.

If we replace B with any convex set, this scheme still works to create a volume preserving map F with divergence at least n. The details of this construction of were worked out by Brothers and Morgan in [3]. They also provide a version of the divergence theorem with weakened hypotheses and show that F satisfies these.

4.3 Paired calibration

In 1993, Lawlor and Morgan [18] gave a simple proof that in every dimension, the cone over the $(n-2)$-skeleton of the regular simplex is area-minimizing. In $\mathbb{R}^2$ this is the length-minimizing Y-shaped figure of three edges meeting at 120-degrees, and in $\mathbb{R}^3$ it is the union of isosceles triangles from each edge of a regular tetrahedron in to its center of mass. This result had already been proved by Jean Taylor in 1975 [23] for $\mathbb{R}^3$. However, the result by Lawlor and Morgan was new in higher dimensions.

A simple description of their "paired calibration" technique is to line up (in $\mathbb{R}^3$, say) four heat lamps shining directly toward the faces of a regular tetrahedron. Consider that the heat rays from

a lamp are parallel with constant intensity, and are completely absorbed when they hit a surface. Now place the proposed minimizing cone in this configuration for a set time, and measure the temperature at each point of the cone. Replace the cone with any competing surface for the same amount of time, and measure its temperature. Because each piece of the cone has the ideal surface angle at which to absorb heat from the two lamps that shine on that piece (analogous to facing a single lamp at 90 degrees), we know that the cone is at least as hot, pointwise, as the competing surface. On the other hand, because both competitors span the same boundary, the total heat absorbed is the same for both. Equal heat absorbed and hotter temperature pointwise means the cone must have less surface area over which to distribute the heat. This approach is made rigorous by representing heat absorbtion by the flux integrals of a set of constant vector fields.

We will combine the Knothe-Gromov vector field approach with paired calibration.

4.4 The Surfaces

A uniform polytope in $\mathbb{R}^n$ (or uniform polyhedron in $\mathbb{R}^3$) is a polytope with symmetric vertices made of unform polytope facets of one dimension down. The uniform polytopes in two dimensions are the regular polygons. In particular the edges of a unform polytope are all of equal length, and the vertices of a unform polytope all have equal distance from its center of mass. Examples of uniform polyhedra in $\mathbb{R}^3$ include the Platonic and Archimedean solids.

Definition 4.4.1 (A family of soap-film-like surfaces with enclosed volume)**.** Let Γ be a convex uniform polytope of dimension $m \leq n$ of unit edge length embedded in $\mathbb{R}^n$ and centered at the origin. Let $\mathbf{p}_1, \ldots, \mathbf{p}_k$ be the vertices of Γ. Then $\sum_i \mathbf{p}_i = \mathbf{0}$ and $\|\mathbf{p}_i - \mathbf{p}_j\| = 1$ for all vertices $\mathbf{p}_i$ and $\mathbf{p}_j$ that are adjacent in Γ.

For each $\mathbf{p}_i$ let C_i be the set of points of $\mathbb{R}^n$ lying strictly closer to $\mathbf{p}_i$ than to any other $\mathbf{p}_j$, and define K to be the complement of $\bigcup C_i$ (if $k = 1$ let $K = \emptyset$). We note then that C_i and C_j share

boundary non-trivially (on a set of non-zero $\mathscr{H}^{n-1}$ measure) if and only if $\mathbf{p}_i$ and $\mathbf{p}_j$ are adjacent vertices in Γ.

Next, choose $r \geq 0$ and define B as the intersection of the open balls of radius r centered at $-r\,\mathbf{p}_i$. Let S be the boundary of B and β the volume of B.

Finally, define

$$M = M(\Gamma, r) = (K \setminus \overline{B}) \cup S.$$

Figure 4.1 contains examples of M for various polytopes Γ. We note that in our construction the faces of B correspond to the vertices of Γ and the vertices of B correspond to the faces of Γ. Thus when this construction is applied to a uniform polytope Γ, the bubble B will be homeomorphic to the dual polytope of Γ. This is why the bubble resulting from Γ = an icosahedron in Figure 4.1 looks like a dodecagon.

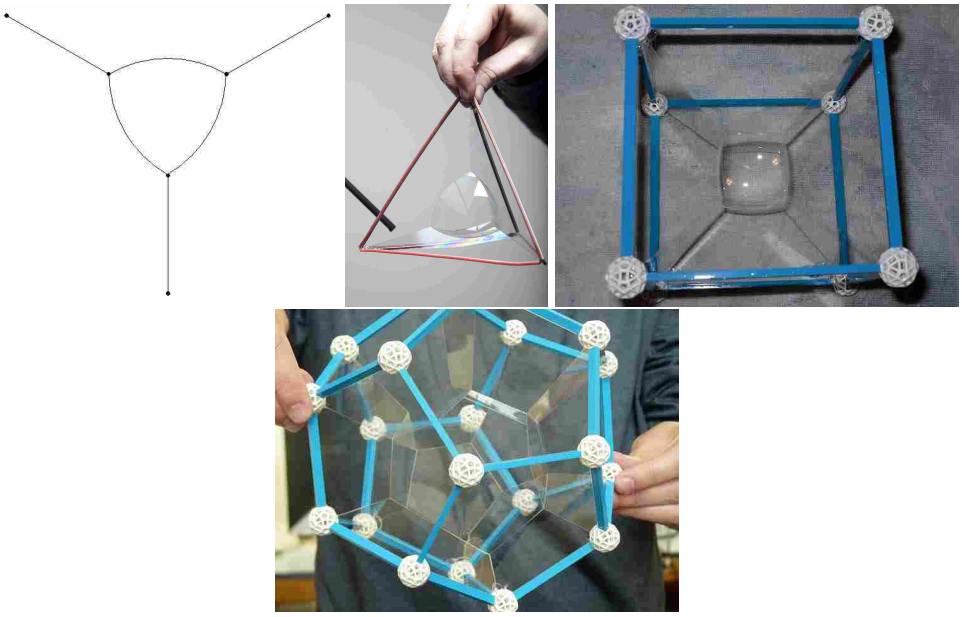

Figure 4.1 Examples of M for $\Gamma =$ an equilateral triangle, a regular tetrahedron, a regular octahedron, a regular icosahedron

Remark 4.4.2. As $\|\mathbf{p}_i\| = \|\mathbf{p}_j\|$ for all i, j, we see that $B = \emptyset$ if and only if $\|\mathbf{p}_i\| < 1$ or $r = 0$. If this

is the case $M = K$ and any volume constraint is vacuous. The proof below will apply to either case. Convex regular polytopes for which $\|\mathbf{p}_i\| < 1$ and this construction may yield a non-empty bubble B include ($m = 2$) k-gons with $k < 6$, ($m = 3$) all platonic solids save the regular dodecahedron, and ($m \geq 4$) the m-simplex and the m-orthoplex. Minimizers over convex uniform polytopes such that $\|\mathbf{p}_i\| \geq 1$ also exist, but need not be convex or have spherical caps as faces.

4.5 The Minimization Theorem

Theorem 4.5.1. *Given Γ and $r \geq 0$, the surface $M = M(\Gamma, r)$ is area-minimizing, in the following sense.*

Let L_0 be the closure of a bounded open set in $\mathbb{R}^n$ such that $M_0 = M \cap L_0$ contains all of S. Let T be any compact surface (rectifiable set) such that

$$(M \setminus M_0) \cup T$$

divides $\mathbb{R}^n$ into k unbounded components T_i such that $C_i \setminus L_0 \subset T_i$ and T_i and T_j share boundary non-trivially only if $\mathbf{p}_i$ is adjacent to $\mathbf{p}_j$ in Γ. Let U be the union of the compact components, and suppose that the volume of U is β, the same as the volume of B. Then

$$\mathscr{H}^{n-1} M_0 \leq \mathscr{H}^{n-1} T.$$

Proof. Take an arbitrary L_0 and define M_0 as in the statement of the theorem. Choose a competing surface T.

Label the unbounded components of $[(M \setminus M_0) \cup T]^C$ as $T_1, \ldots, T_k$ and label the union of the compact components as U, as in the statement of the theorem. For each i let

$$X_i = \partial U \cap \overline{T_i},$$

and for each $i \neq j$ let

$$W_{ij} = (\partial T_i) \cap (\partial T_j) \cap L_0.$$

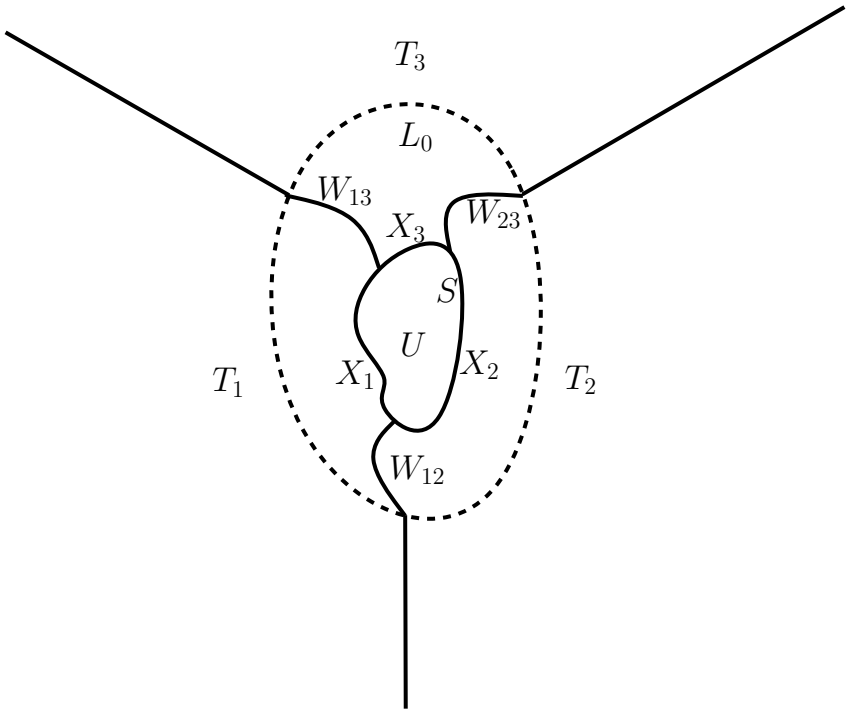

Figure 4.2 Illustration of Labeling ($n = 2$, $k = 3$)

Note then that $\mathscr{H}^{n-1}W_{ij} \neq 0$ only if $\mathbf{p}_i$ and $\mathbf{p}_j$ are adjacent in Γ. This labeling is illustrated in an example in Figure 4.2.

For each point $\mathbf{p}_i$ define a constant vector field $\mathbf{v}_i(\mathbf{x}) = \mathbf{p}_i$.

Use the Knothe/Gromov approach to define a volume-preserving map F from U to the convex set B, with $\operatorname{div} F \geq n$ wherever defined. Think of the map $\frac{1}{r}F$ as a vector field on U, so that

$$\operatorname{div} \frac{1}{r}F \geq \frac{n}{r}.$$

Notice now that every point $\mathbf{y} \in B$ is within distance r of $-r\mathbf{p}_i$ for all $1 \leq i \leq k$, which implies that $\left\| \frac{1}{r}\mathbf{y} + \mathbf{p}_i \right\| \leq 1$. So we see that the sum of vectors $\frac{1}{r}F + \mathbf{v}_i$ has length at most 1 anywhere. Recall that the difference vectors $\mathbf{v}_i - \mathbf{v}_j = \mathbf{p}_i - \mathbf{p}_j$ are also of length 1 on W_{ij} if W_{ij} has non-zero measure. From this point on, we ignore all W_{ij} of measure zero. Let us establish the convention that the (unit) normal $\mathbf{n}_0$ to ∂U is outward pointing, and the normal $\mathbf{n}_{ij}$ to W_{ij} points toward the

region with lower index. We may now compute:

$$\mathscr{H}^{n-1}T = \int_{\partial U} 1 + \sum_{i<j} \int_{W_{ij}} 1 \tag{4.1}$$

$$\geq \sum_i \int_{X_i} \left(\frac{1}{r} F + \mathbf{v}_i \right) \cdot \mathbf{n}_0 + \sum_{i<j} \int_{W_{ij}} \left(\mathbf{v}_i - \mathbf{v}_j \right) \cdot \mathbf{n}_{ij} \tag{4.2}$$

We wish to rewrite (4.2) by considering the flux into the region T_i due to $\mathbf{v}_i$. This is the flux through $\partial T_i \cap T = \left(\bigcup_i W_{ij} \right) \cup X_i$, with normal $\mathbf{n}_i$ pointing into T_i. From the first sum we have the contribution of $\mathbf{v}_i$ through X_i. For each j we also have flux through W_{ij} from the second sum. Notice that if $i < j$, then $\mathbf{n}_{ij} = \mathbf{n}_i$, while if $i > j$, then $\mathbf{n}_{ij} = -\mathbf{n}_i$. Thus we may rewrite (4.2) as

$$\int_{\partial U} \frac{1}{r} F \cdot \mathbf{n}_0 + \sum_i \int_{\partial T_i \cap T} \mathbf{v}_i \cdot \mathbf{n}_i \tag{4.3}$$

$$= \int_U \operatorname{div} \frac{1}{r} F + \sum_i \int_{\partial T_i \cap T} \mathbf{v}_i \cdot \mathbf{n}_i \tag{4.4}$$

$$\geq \frac{n}{r} \text{Volume}(U) + \sum_i \int_{\partial T_i \cap T} \mathbf{v}_i \cdot \mathbf{n}_i. \tag{4.5}$$

Notice that any term in the sum in (4.5) is the flux of a constant vector field through a surface with fixed boundary. We see then that the quantity (4.5) is independent of T (with L_0 held constant).

We claim that equality holds throughout when we apply this estimate to the conjectured minimal surface. When $T = M_0$, we have $F(\mathbf{x}) = \mathbf{x}$. The inward pointing unit normal to X_i at $\mathbf{x}$ is given by $\frac{1}{r}\mathbf{x} + \mathbf{p}_i = \frac{1}{r}F(\mathbf{x}) + \mathbf{v}_i$. Also, notice that W_{ij} consists of points equidistant from $\mathbf{p}_i$ and $\mathbf{p}_j$, so if $i < j$, the normal to W_{ij} is given by $\mathbf{p}_i - \mathbf{p}_j$. This shows that we have equality from (4.1) to (4.2). Also notice that if F is the identity function, then $\operatorname{div} F = n$, giving us equality in the last step (4.5).

Letting $G(T) = \sum_i \int_{X_i} \left(\frac{1}{r} F + \mathbf{v}_i \right) \cdot \mathbf{n}_0 + \sum_{i<j} \int_{W_{ij}} \left(\mathbf{v}_i - \mathbf{v}_j \right) \cdot \mathbf{n}_{ij}$ from (4.2) above, we see that this argument reduces to a proof that

$$\mathscr{H}^{n-1}T \geq G(T) \geq G(M_0) = \mathscr{H}^{n-1}M_0.$$

□

We have shown that M_0 is mass minimizing among all figures that contain the same volume, have the same boundary, and have the same connectivity (regions T_i and T_j for some competitor T share boundary non-trivially only if they do in M_0). If Γ is a regular simplex then, as Γ is also a complete graph, T_i shares non-trivial boundary in M_0 with all other T_j. Thus we have the following corollary:

Corollary 4.5.2. *If Γ is a regular simplex, then M_0 is minimizing as above but without the connectivity condition.*

It is an open problem however as to which figures $M(\Gamma, r)$ other than those generated from a regular simplex are minimizing in this more general setting.

Corollary 4.5.3. *If Γ' is the dual polytope to some convex uniform polytope Γ, then the cone over Γ' is minimizing among all other surfaces that share the same boundary and have the same connectivity.*

Proof. Apply Theorem 4.5.1 to $M(\Gamma, 0)$. □

The above corollary is a stronger version of the main result of [4], which showed that stationary cones are minimizing over diffeomorphisms. Choe's results however apply to the more general class of polyhedral sets, and not just cones.

4.6 Metacalibration

The proof of Theorem 4.5.1 is an example of a method which we call *metacalibration*. Calibration arguments [12] typically have the form

$$\mathscr{H}^n M = \int_M \varphi = \int_{M'} \varphi \leq \mathscr{H}^n M'$$

for some particular differential form φ, showing that M is mass minimizing among all competitors M'. This method has been useful in solving fixed boundary problems, such as Plateau's problem

(see [20], c.f. chapter 6). Metacalibration generalizes the traditional calibration argument by allowing φ to vary for each competitor. This allows metacalibration to tackle problems with fixed volume constraints. As demonstrated in this paper, metacalibration can also handle combinations of fixed boundary and fixed volume constraints.

Using a variation of the Knothe-Rosenblatt rearrangement in a metacalibration argument, the authors were able to prove the double bubble conjecture in the plane [9]. Optimal transport promises to be another promising tool for constructing metacalibrations. For instance, the Brenier map [2] has many of the same properties of as the Knothe-Rosenblatt rearrangement, including the divergence criterion used in this paper. We hope that a suitable generalization of the Brenier map can be used to solve other isoperimetric problems such as the triple bubble conjecture.

Chapter 5

Soap Film Realization of Isoperimetric Surfaces with Boundary: By Jacob Ross, Donald Sampson, and Neil Steinburg

We examine surfaces of the type proved to be minimizing under a connectivity condition by Dorff et al. in "Isoperimetric Surfaces with Boundary". We determine which of these surfaces are stable soap films. The connectivity condition is shown to be very restrictive; few of these surfaces are stable (locally minimizing) without it.

5.1 Introduction

Surface area minimization in soap bubbles and soap films is one of the more fascinating subjects in mathematics today. Metacalibration techniques (a generalization of the calibrations popularized by Harvey and Lawson [12], see also [20], cf. chapter 6) were developed to investigate the problems that arise in surface minimization. In particular metacalibration techniques prove very useful in solving a new class of problems with both fixed volume and fixed boundary constraints. We call

these problems *equitent problems* after Lawlor et al. Equitent stands for equal content (volume condition) and equal extent (boundary condition). [7]

In this paper we consider a certain class of equitent problems addressed in "Isoperimetric Surfaces with Boundary" [8]. Dorff et al. show that certain equitent surfaces are globally minimizing under a connectivity condition that restricts the surfaces' homotopy class. This connectivity condition is not however true for general minimizing surfaces. We examine which of these surfaces are locally minimizing without the connectivity condition. This is equivalent to showing these surfaces are realizable as a soap film. We demonstrate this for those surfaces that are proved to be locally minimal.

5.2 The Surfaces of Dorff et al.

The surfaces under consideration are described as the union of sections of spheres and planes. They are constructed by starting with a cone over a wire frame polyhedron. The center of the cone is then replaced by a volume (bubble) that is enclosed by spherical caps in the same polyhedral arrangement. See the example soap film in Figure 5.1.

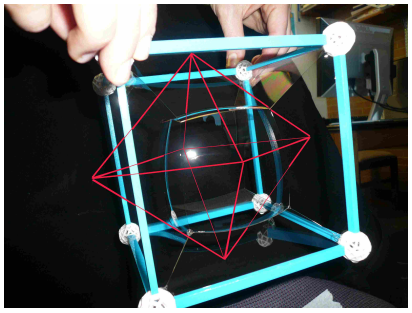

Figure 5.1 Equitent surface constructed on a cube wireframe

Dorff et al. categorize these figures by defining a *connectivity graph*. The connectivity graph is used in the construction of these surfaces and describes the adjacency conditions on the resulting surface. The wire frame polyhedron is the dual figure to this connectivity graph. In their paper

Dorff et al. also define a connectivity condition, which is that exterior regions share boundary only if the corresponding vertices in the connectivity graph are adjacent. They prove that the constructed surfaces are globally area minimizing among all surfaces that enclose the same fixed volume, have the same wire frame polyhedral boundary, and satisfy the connectivity condition.

5.3 Soap Film Stability

The following is our main result.

Theorem 5.3.1. *Among all the minimal surfaces of Dorff et al. in $\mathbb{R}^3$, there are only six that are stable as a soap film: those whose connectivity graphs are a single point, edge, equilateral triangle, regular tetrahedron, regular octahedron, or regular icosahedron.*

Proof. We relax the connectivity condition and look at which surfaces are locally area minimizing among surfaces that enclose the same fixed volume and have the same wire frame polyhedral boundary. We reduce conditions for local minimality to conditions on the connectivity graph.

First, in the constuction of the surfaces Dorff et al. require that the connectivity graph to be a uniform polyhedron (polytope) of unit edge length. A uniform polyhedron is one with regular polygon faces and congruent vertices. This guarantees the existence of particular vector fields needed in the minimization proof. They also require the circumradius of the connectivity graph to be strictly less than 1. A circumradius greater than or equal to 1 would create a central bubble of volume zero. Uniform polyhedra that meet this condition are limited to the tetrahedron, cube, octahedron, icosahedron, triangular prism, pentagonal prism, square antiprism, and pentagonal antiprism.

Minimality conditions come from the work of Jean Taylor [23]. She proved that Plateau's rules for soap films must hold for locally minimizing surfaces in $\mathbb{R}^3$. These are:

1. Soap films are made of smooth surfaces of constant mean curvature.

2. Soap films always meet in threes along a smooth curve, meeting at equal angles of 120^o.

3. These curves meet in fours at a point, meeting at equal angles of $\cos^{-1}(-\frac{1}{3})$ (approximately 109^o).

The first and third rules always hold as a result of the surface's construction. The second rule, however, further limits the number of connectivity graphs that can be formed. In the construction, each face of the connectivity graph corresponds to one of these curves (from a vertex of the wire-frame polyhedron) and each edge corresponds to a smooth surface connecting to this curve (from an edge of the wire-frame polyhedron). Thus the second rule implies that connectivity graphs must be constrained to have only triangular faces.

The uniform polyhedra that meet the conditions on the construction and satisfy this second rule are limited to the tetrahedron, octahedron, and icosahedron. For connectivity graphs in lower dimensions that also satisfy these conditions, we have a single point (0 dimensions), a line segment (1 dimension), and an equilateral triangle (2 dimensions). □

These conditions are very restrictive; out of the 18 convex uniform polyhedrons and infinite sets of prisms, antiprisms, and lower dimensional figures, only six equitent surfaces can be created in $\mathbb{R}^3$. In the next section we demonstrate each of these surfaces as a soap film.

5.4 Realization of the Bubbles

Equitent surfaces can be realized as a soap film by dipping a wire-frame in a soap solution and blowing a soap bubble onto the surface. (It may however take several tries to get a surface of a particular homotopy class, and have it last long enough to take a picture!) Each of the six connectivity graphs identified in the last section do generate a stable minimal surface when realized as a soap film this way. Note that the wire-frame polyhedron in each case is the dual figure to the

connectivity graph. Also note that the number of vertices in the connectivity graph corresponds to the number of exterior regions separated by the equitent surface.

For lower dimensional connectivity graphs we see that the surface realized from a single point is a spherical bubble with no wire frame (5.2(a)). A single edge as a connectivity graph yields a lens shaped bubble on a planar surface. Here we represent the wire-frame as a circle (any polygon in 2 dimensions will do). (5.2(b)). From an equilateral triangle we have a 'football' shaped bubble connected to three planar surfaces (5.2(c)).

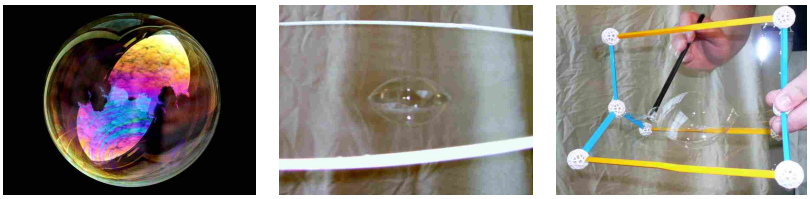

(a) Dimension 0 (b) Dimension 1 (c) Dimension 2

Figure 5.2 Equitent surfaces with lower dimensional connectivity graph

For the three dimensional connectivity graphs, a polyhedral shaped bubble with spherical caps will be formed. These figures will also have planar surfaces connecting to each edge of the bubble. For tetrahedral, octahedral, or icosahedral connectivity graphs we get a tetrahedron (5.3(a)), cube (5.3(b)), or dodecahedron (5.3(c)) shaped bubble respectively.

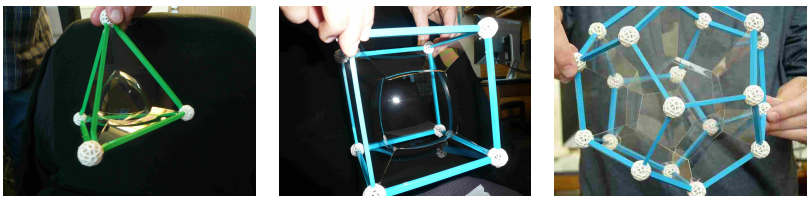

(a) Tetrahedral graph (b) Octahedral graph (c) Icosahedral graph

Figure 5.3 Equitent surfaces with dimension 3 connectivity graph

5.5 Conclusion

As noted earlier, we have seen that the connectivity condition of Dorff et al. is a very restrictive condition. Each of the locally minimizing surfaces were known prior to their work, though perhaps not yet proven to be minimal. The real impact of their paper comes from the pioneering new method of metacalibration and how we can use it to tackle equitent problems. Their paper gives the first new results proven using this method, though it has also been used to provide new proofs of some multiple bubble problems [6].

We hope to be able to generalize the metacalibration approach to handle further equitent problems. This includes finding an alternate construction of equitent surfaces that relaxes the uniformity condition on the connectivity graphs. This would allow us to investigate surfaces such as those generated on a rectangular prism wire-frame, not just a cube (see Figure 5.4(a)).

Another problem to consider are equitent surfaces that would be generated by connectivity graphs of circumradius greater than or equal to 1. Such surfaces are stable in $\mathbb{R}^2$ and $\mathbb{R}^3$, though the central bubble has negative pressure and the faces bow inwards (see Figure 5.4(b)).

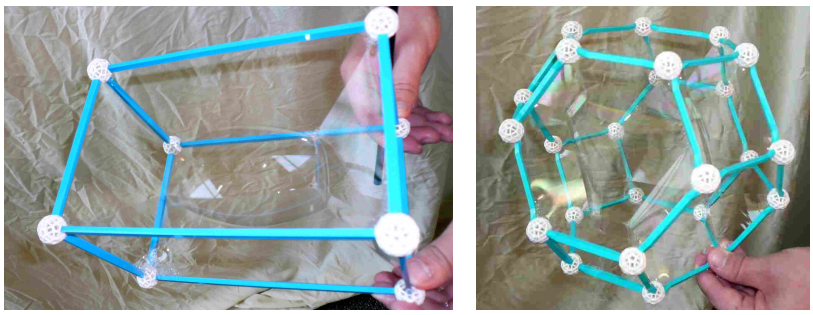

(a) Rectangular prism wire-frame (b) Negative pressure soap bubbles

Figure 5.4 Other examples of equitent surfaces

Chapter 6

Isoperimetric Surfaces with Boundary II: By Abraham Frandsen, Donald Sampson, and Neil Steinburg

Following our previous work with Dorff and Lawlor, we extend results for the so-called equitent problem of fixed boundary and fixed volume. We define sufficient conditions, which in $\mathbb{R}^2$ and $\mathbb{R}^3$ are also necessary, for local minima to be piecewise spherical, and we show that these are area-minimizing in their homotopy class. We also give new examples of these surfaces in $\mathbb{R}^2$ and $\mathbb{R}^3$.

6.1 Introduction

Equitent problems, first introduced in "Isoperimetric Surfaces with Boundary," [8] ask what is the area minimizing surface enclosing a given volume and spanning a given boundary. In this way, equitent problems represent a combination of isoperimetry and boundary conditions, such as in Steiner problems and minimal surfaces. Our previous approach, which we extend here, uses the

technique of metacalibration. *Metacalibration* is a version of the calibration methods popularized by Harvey and Lawson [12] adapted to use on isoperimetric problems. In particular, we use a combination of the mapping of Gromov [11], after Knothe [16], and the paired calibrations of Lawlor and Morgan [18].

In our original results, we construct various classes of surfaces bounded by the dual figures of uniform polytopes and enclosing a prescribed volume and prove that these surfaces are minimizing in their homotopy class. The results, however, turn out to be limited in scope, as Ross et al. show in their paper "Soap Film Realization of Isoperimetric Surfaces with Boundary" [15]. Consequently, there remains much ground to be covered.

In this paper, we will extend previous results by considering equitent systems generated by polytopes whose edges are all of a given length. This results in a much wider range of equitent surfaces than those bounded by uniform polytopes. We construct the conjectured minimizing surface using a refinement of previous methods and prove that this surface is indeed area-minimizing in its homotopy class.

Further, we show that any homotopically area-minimizing equitent surface with piecewise spherical faces and simplex vertex figures is equivalent to one generated by our construction. We conclude with a discussion of new equitent surfaces and a survey of open problems.

6.2 The Surfaces

Let Γ be a convex polytope of dimension $m \leq n$ with equal edge lengths, r, embedded in $\mathbb{R}^n$. Let $p_1, \ldots, p_k$ be the vertices of Γ. For each p_i let $R_i = \{x \in \mathbb{R}^n : ||x - p_j|| < ||x - p_i||$, for all $j \neq i, r < ||x - p_i||\}$ (the region farthest from p_i). Note that if p_i and p_j share an edge in Γ, $\partial R_i \cap \partial R_j$ is a subset of the perpendicular bisecting hyperplane of that edge. Now, define $R_0 = \{x \in \mathbb{R}^n : ||x - p_i|| < r, 1 \leq i \leq k\}$. See below. This region represents the enclosed volume. We suppose that

$R_0 \neq \emptyset$ and $\mathscr{H}^{n-1}(\partial R_0 \cap \partial R_i) \neq 0$ for all $i > 0$. Let $V_0 = \mathscr{H}^n(R_0)$. Then let $M = \bigcup_{i=0}^{k} \partial R_i$.

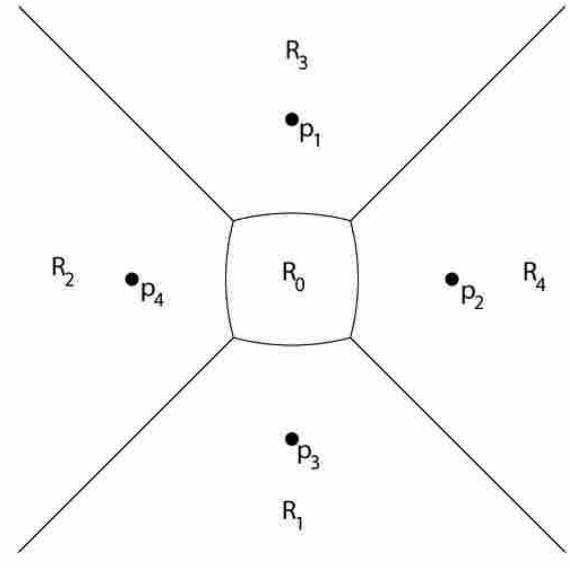

Notice that ∂R_0 is the portion of the surface that encloses the volume R_0. In order to have a nontrivial result, we require $R_0 \neq \emptyset$. The condition $\mathscr{H}^{n-1}(\partial R_0 \cap \partial R_i) \neq 0$ for all $i > 0$ ensures that all smooth subsurfaces of M meet at 120 degree angles. For $m = 2$, the only viable generating figures, Γ, are equilateral triangles, rhombi with interior angles strictly greater than 60°, and small perturbations of regular pentagons. For $m = 3$, the valid generating figures include all but two of the eight convex deltahedra (polyhedra where all faces are equilateral triangles), as well as other polytopes with faces of higher degree. It is worth noting, however, that those generating figures, Γ, whose faces are not equilateral triangles produce surfaces which are locally minimal within their homotopy class, but not globally minimal. As will be seen in the proof, this construction gives sufficient conditions for minimizing surfaces to be piecewise spherical. Furthermore, due to the regularity properties of soap films proved by Taylor and Almgren [23], these are also necessary conditions in $\mathbb{R}^2$ and $\mathbb{R}^3$. In higher dimensions non-simplicial vertex figures may be minimizing, but are not considered in this paper. See for example [1].

6.3 The Minimization Theorem

In this section we prove that the surfaces constructed are homotopically minimizing in the following sense: Let U be a bounded open set that contains $\overline{R_0}$, and let $M_0 = M \cap U$.

Theorem 6.3.1. *The surface M_0 is surface area minimizing among all compact surfaces (rectifiable sets) in U with boundary $\partial U \cap M$ that enclose the fixed volume $\mathscr{H}^n(R_0)$ and are homotopically equivalent to M_0. This also holds with the weaker assumption that competitor surfaces are not nessisarily homotopic to M_0 but separate space into the same regions as M_0 and these regions share boundary non-trivially (on a set of positive $\mathscr{H}^{n-1}$ measure) only if the corresponding regions do in M_0.*

Our proof uses a metacalibration argument that compares figures according to their flux on specially crafted vector fields. In particular, we use a paired-calibration approach with one vector field defined for each separated region.

Let N be any competitor surface and let S_i be the separated regions that correspond to each R_i respectively. (Then $\mathscr{H}^n(S_0) = \mathscr{H}^n(R_0)$ by the volume condition.) Define $v_i : S_i \to \mathbb{R}^n$ for $1 \leq i \leq m$ to be the constant vector field $-\frac{p_i}{r}$. Let $\phi : S_0 \to R_0$ be the Knothe-Rosenblatt rearrangement and let $v_0 : S_0 \to \mathbb{R}^n$ be given by $v_0 = \frac{\phi}{r}$.

At this point a few simple results would be useful:

Proposition 6.3.2. *If S_i and S_j share boundary non-trivially, then $v_i - v_j$ is a unit vector. If $N = M_0$ then $v_i - v_j$ is the unit normal to $\partial R_i \cap \partial R_j$.*

Proof. Note that S_i and S_j share boundary non-trivially if and only if p_i and p_j are adjacent in Γ. Thus $||v_i - v_j|| = \frac{1}{r}||p_i - p_j|| = 1$. Also if $N = M_0$, $v_i - v_j$ is the unit normal to $\partial R_i \cap \partial R_j$ since $\partial R_i \cap \partial R_j$ lies on the hyperplane equidistant to p_i and p_j. □

Proposition 6.3.3. *The matrix Dv_0 is triangular. If $N = M$ then v_0 is the identity scaled by $\frac{1}{r}$.*

Proof. Follows from the definition of v_0. See [8] for details. □

Proposition 6.3.4. *For $i \neq 0$, $\int_{N\cap\partial S_i} v_i \cdot n\, d\mathscr{H}^{n-1} = \int_{M\cap\partial R_i} v_i \cdot n\, d\mathscr{H}^{n-1}$, where n is the unit normal to the surface of integration, outward pointing with respect to S_i or R_i.*

Proof. Follows from the divergence theorem since v_i is divergence free and $\partial(M\cap\partial R_i) = \partial(N\cap\partial S_i)$. □

We now complete the proof of Theorem 6.3.1.

Proof. For any competitor surface N, let $G(N) = \sum_i \int_{N\cap\partial S_i} v_i \cdot n\, d\mathscr{H}^{n-1}$. Letting $P(N) = \sum_i \int_{N\cap\partial S_i} d\mathscr{H}^{n-1}$ be our objective function, we find that

$$\begin{aligned}
G(N) &= \sum_i \int_{N\cap\partial S_i} v_i \cdot n\, d\mathscr{H}^{n-1} \\
&= \sum_{i\neq j} \int_{N\cap(\partial S_i\cap\partial S_j)} (v_i - v_j)\cdot n\, d\mathscr{H}^{n-1} \\
&\leq \sum_{i\neq j} \int_{N\cap(\partial S_i\cap\partial S_j)} ||v_i - v_j||||n||\, d\mathscr{H}^{n-1} \\
&\leq \sum_{i\neq j} \int_{N\cap(\partial S_i\cap\partial S_j)} d\mathscr{H}^{n-1} \\
&= \sum_i \int_{N\cap\partial S_i} d\mathscr{H}^{n-1} = P(N),
\end{aligned}$$

with equality if $N = M_0$.

Now also note that

$$\begin{aligned}
\int_{N\cap\partial S_0} v_0 \cdot n\, d\mathscr{H}^{n-1} &= \int_{S_0} \mathrm{div} v_0\, d\mathscr{H}^{n-1} \\
&= \int_{S_0} \frac{1}{r}\left(\frac{\partial\phi_1}{\partial x_1} + \frac{\partial\phi_2}{\partial x_2} + \cdots + \frac{\partial\phi_n}{\partial x_n}\right) d\mathscr{H}^{n-1} \\
&\geq \int_{S_0} \frac{n}{r}\sqrt[n]{\frac{\partial\phi_1}{\partial x_1}\frac{\partial\phi_2}{\partial x_2}\cdots\frac{\partial\phi_n}{\partial x_n}}\, d\mathscr{H}^{n-1} \\
&= \int_{S_0} \frac{n}{r}\sqrt[n]{1}\, d\mathscr{H}^{n-1} \\
&= \frac{n}{r}\mathscr{H}^{n-1}(S_0) = \frac{n}{r}\mathscr{H}^{n-1}(R_0),
\end{aligned}$$

with equality if $N = M_0$. This follows from the AM-GM inequality and the equality $\frac{\partial \phi_1}{\partial x_1}\frac{\partial \phi_2}{\partial x_2}\cdots\frac{\partial \phi_n}{\partial x_n} = \det(D\phi) = 1$, since ϕ is volume preserving.

Combining these results we find

$$\begin{aligned} P(M_0) = G(M_0) &= \sum_{i\neq 0}\int_{M_0\cap\partial R_i} v_i \cdot n\, d\mathscr{H}^{n-1} + \int_{M_0\cap\partial R_0} v_0 \cdot n\, d\mathscr{H}^{n-1} \\ &= \sum_{i\neq 0}\int_{N\cap\partial S_i} v_i \cdot n\, d\mathscr{H}^{n-1} + \frac{n}{r}\mathscr{H}^{n-1}(R_0) \\ &\leq \sum_{i\neq 0}\int_{N\cap\partial S_i} v_i \cdot n\, d\mathscr{H}^{n-1} + \int_{N\cap\partial S_0} v_0 \cdot n\, d\mathscr{H}^{n-1} \\ &= G(N) \leq P(N). \end{aligned}$$

□

6.4 Soap films in $\mathbb{R}^3$

In [8], [15] we identified the regular tetrahedron, the regular octahedron, and the regular icosahedron as polytopes that generate realizable soap films. The only other three-dimensional polytopes, Γ, that generate surfaces realizable as soap films are the triangular dipyramid, the pentagonal dipyramid, and the snub disphenoid. The generated soap films are shown below.

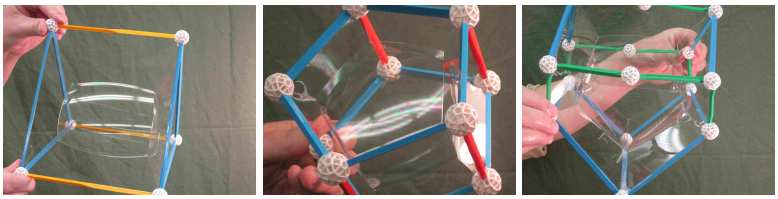

This is due to the conditions proven by Jean Taylor in [23], namely that each face not intersecting with the boundary must meet with exactly two other faces in 120-degree angles. Thus, any generating figure, Γ, with non-triangular faces will not yield a surface realizable as a soap film. The remaining two deltahedra fail to meet the conditions of our construction because of their large circumradius.

Every surface generated by our construction will have piecewise spherical faces and simplicial vertex figures. The converse is also true. Given any area-minimizing equitent surface with piecewise spherical faces and simplicial vertex figures, we can recover the generating polytope, Γ, as the set of centers of each spherical face. In higher dimensions there may exist area minimizing equitent surfaces with non-simplicial vertex figures.

6.5 Conclusion

In this paper we have characterized all piecewise-spherical equitent surfaces in two and three dimensions, and proven them to be area minimizing. Several interesting and open problems arise. An especially intriguing question deals with equitent surfaces that have negatively curved bubbles, meaning each face of the bubble region bends inward. Such a surface can be created using soap films, but our methods are not yet able to address this case. Similarly, equitent surfaces with non-spherical faces fall outside the scope of our approach. Finally, our construction generates surfaces whose vertices are cones over simplices. In spaces of dimension greater than three, however, minimal surfaces need not have simplicial vertex figures, and we may yet find interesting new equitent surfaces. Extensions of the metacalibration methods outlined in this paper show great promise in solving these open problems.

Part IV

A Note on Metacalibration Maps

Chapter 7

Metacalibration Maps

7.1 Unification of Previous Methods

As mentioned previously in Section 3.1, metacalibration provides a strong tool for unifying a variety of approaches to proving the isoperimetric inequality. While the result is the same in each case, each approach is in essence using a subtly different metacalibration function. Since each approach is unique and has both positive and negative aspects it is appropriate to mention a little about them.

The clearest application of metacalibration comes from Gromov's proof of the isoperimetric inequality [11] in arbitrary dimension. As mentioned several times above, this proof relies on the Knothe-Rosenblatt rearrangement (see [16], [22]). For simplicity, we may say that this rearrangement matches both the total volume and 'volume under a slice' of the competitor figure. While the simplest in application, this approach relies on mapping straight lines through the figure. This can get difficult, however, when we try to map more complicated figures or spaces (see Chapter 3).

Gary Lawlor also made a nice adaptation of the Knothe-Rosenblatt rearrangement to prove the isoperimetric inequality. While using the same rearrangement as Gromov, Lawlor altered the

metacalibration so that $G(\Omega^*) = G(\Omega)$ for all competitors Ω. One benefit of this approach is that it can be simplified to use only first-year, one-variable calculus. The drawback is that it is difficult to generalize to dimensions higher than two.

Under advisement from Lawlor, my colleague James Dilts created a new metacalibration approach [5] that we affectionately named the τ-method. His metacalibration map matches the volume under a slice, but matches the area of the slice instead of the total volume, letting the image space vary. This allows the application of this approach to spaces with metrics constant along parallel lines. Successful proofs have been given this way for the isoperimetric inequality in spherical and hyperbolic spaces.

One interesting and unexpected application of metacalibration was found in Schmidt's proof of the isoperimetric inequality [21]. At first glance the proof is hard to relate to a metacalibration approach. Noting however that the crux of the argument relies on Green's theorem, we can rearrange terms to show that Schmidt is in effect using a rearrangement that preserves the total height of the figure and the height of each slice. It is a very elegant proof and an excellent example of Green's theorem for students of multivariate calculus, but it also has no natural generalization to dimensions higher than two.

As opposed to all other approaches, Robert McCann gave a unique version of the isoperimetric inequality [19] in that the rearrangement used was not found constructively. Previously, Yann Brenier found that any volume preserving map between spaces can be 'factored' into a composition of maps in which one is the gradient of a convex function [2]. This map was found as the solution to an optimal transport problem, which was previously proven (non-constructively) to exist. McCann used this map as the basis of his metacalibration function to complete a very short and elegant proof of the isoperimetric inequality.

7.2 New Methods

With the wide variety of rearrangements that can be used in a metacalibration framework, it is not surprising to expect there to be many more. With each having its own drawbacks and strengths, we should be able to find some map that will be able to work in almost any situation. The non-constructive approach using optimal transport seems especially promising in this regard for creating maps with the specific properties needed in a variety of isoperimetric problems. Believing these maps to exist, the next chapter describes what could be done once they are found.

Chapter 8

Maps with Boundary Control

8.1 A Conjecture

Over the past few years my faith in the beauty of mathematics has led me to believe that there must exist some metacalibration map that has some control on how the boundary of a competitor figure gets mapped. One example of how this might look is the following:

Conjecture 8.1.1. *Given any figure* $\Omega = \Omega_1 \cup \Omega_2 \cup \cdots \cup \Omega_m \subset \mathbb{R}^n$, *let* $\Omega^* = \Omega_1^* \cup \Omega_2^* \cup \cdots \cup \Omega_m^* \subset \mathbb{R}^n$ *be a conjectured minimizer such that* $\mathrm{Vol}^n(\Omega_i) = \mathrm{Vol}^n(\Omega_i^*)$ *for all* $1 \leq i \leq m$. *Given a separation of* $\partial\Omega$ *into regions* $R_1, R_2, \ldots, R_k$ *and a corresponding separation of* $\partial\Omega^*$ *into regions* $R_1^*, R_2^*, \ldots, R_k^*$ *that preserve the adjacency of* $\Omega_i^{(*)}$ *and* $R_j^{(*)}$, *then there exists a map* $\varphi_\Omega : \Omega \to \Omega^*$ *such that* φ_Ω *is volume preserving,* $\operatorname{div} \varphi_\Omega \geq n$, $\varphi_\Omega(\Omega_i) = \Omega_i^*$ *for all* $1 \leq i \leq m$, *and* $\varphi_\Omega(R_j) = R_j^*$ *for all* $1 \leq j \leq k$.

With a proof of this conjecture, a wide variety of results could be easily obtained.

8.2 Equitent Problems

For all three papers in Part III we required that all the bubbles in minimizing equitent surfaces have relatively positive pressure with respect to the bubble's exterior (equivalently an inward pointing mean curvature vector). This was generally achieved via some form of circumradius condition or limitation on the bubble's connectivity. This is however merely an artifact of not having proper boundary control on the mapping of negatively pressured bubbles.

Take for example the construction in Chapter 6. If we alter the region R_0 to be the bounded component of $\{x \in \mathbb{R}^n : ||x - p_i|| > r, 1 \leq i \leq k\}$ and let $v_i : S_i \to \mathbb{R}^n$ for $1 \leq i \leq m$ to be the constant vector field $+\frac{p_i}{r}$ then the proof follows in exactly the same fashion to show minimization of a bubble with interior pressure $-\frac{1}{r}$. Without the appropriate boundary control however, we would find $||v_0 - v_i|| > 1$ if any point on the boundary of S_0 was mapped away from the corresponding face of R_0.

8.3 Multiple Bubble Problems

With conjecture 8.1.1, proof of the multiple bubble conjecture comes naturally.

Theorem 8.3.1. *The least surface volume way to separately enclose $n+1$ volumes in $\mathbb{R}^n$ is the standard $n+1$-bubble made of parts of spheres.*

Proof. Let $\Omega = \Omega_1 \cup \Omega_2 \cup \cdots \cup \Omega_{n+1}$ be any competitor figure and $\Omega^* = \Omega_1^* \cup \Omega_2^* \cup \cdots \cup \Omega_{n+1}^*$ be the standard $n+1$ bubble of the same volumes. Define the regions in $\partial\Omega$ and $\partial\Omega^*$ to be the exterior boundaries of each bubble, $R_i^{(*)}$, and the interfaces between each pair of bubbles, $R_{ij}^{(*)}$. Given then the existence of φ_Ω, let $G(\Omega) = \sum_i \int_{\partial\Omega_i} \langle \vec{n}, (\varphi_\Omega - o_i)/r_i \rangle d\,\mathrm{Vol}^{n-1}$ where $\vec{n}$ is the unit normal and o_i is the center and r_i the radius of spherical region R_i^*. Then we find the following:

$$
\begin{aligned}
P(\Omega^*) &= \int_{\partial\Omega^*} d\,\mathrm{Vol}^{n-1} \\
&= \sum_i \int_{R_i^*} d\,\mathrm{Vol}^{n-1} + \sum_{i\neq j} \int_{R_{ij}^*} d\,\mathrm{Vol}^{n-1} \\
&= \sum_i \int_{R_i^*} \langle \vec{n}, \frac{\mathrm{id}-o_i}{r_i} \rangle d\,\mathrm{Vol}^{n-1} + \sum_{i\neq j} \int_{R_{ij}^*} \langle \vec{n}, \frac{\mathrm{id}-o_i}{r_i} - \frac{\mathrm{id}-o_j}{r_j} \rangle d\,\mathrm{Vol}^{n-1} \\
&= \sum_i \int_{\partial\Omega_i^*} \langle \vec{n}, \frac{\mathrm{id}-o_i}{r_i} \rangle d\,\mathrm{Vol}^{n-1} = G(\Omega^*) \\
&= \sum_i \int_{\Omega_i^*} \mathrm{div}\, \frac{\mathrm{id}-o_i}{r_i} d\,\mathrm{Vol}^n \\
&= \sum_i \int_{\Omega_i^*} \frac{n}{r_i} d\,\mathrm{Vol}^n \\
&= \sum_i \frac{n}{r_i} \mathrm{Vol}(\Omega_i^*) = \sum_i \frac{n}{r_i} \mathrm{Vol}(\Omega_i) \\
&= \sum_i \int_{\Omega_i} \frac{n}{r_i} d\,\mathrm{Vol}^n \\
&\leq \sum_i \int_{\Omega_i} \mathrm{div}\, \frac{\varphi_\Omega - o_i}{r_i} d\,\mathrm{Vol}^n \\
&= \sum_i \int_{\partial\Omega_i} \langle \vec{n}, \frac{\varphi_\Omega - o_i}{r_i} \rangle d\,\mathrm{Vol}^{n-1} = G(\Omega) \\
&= \sum_i \int_{R_i} \langle \vec{n}, \frac{\varphi_\Omega - o_i}{r_i} \rangle d\,\mathrm{Vol}^{n-1} + \sum_{i\neq j} \int_{R_{ij}} \langle \vec{n}, \frac{\varphi_\Omega - o_i}{r_i} - \frac{\varphi_\Omega - o_j}{r_j} \rangle d\,\mathrm{Vol}^{n-1} \\
&\leq \sum_i \int_{R_i} d\,\mathrm{Vol}^{n-1} + \sum_{i\neq j} \int_{R_{ij}} d\,\mathrm{Vol}^{n-1} \\
&= \int_{\partial\Omega} d\,\mathrm{Vol}^{n-1} = P(\Omega^*)
\end{aligned}
$$

□

Bibliography

[1] Kenneth Brakke. Minimal cones on hypercubes. *J. Geom.*, 1(4):329–338, 1991.

[2] Yann Brenier. Polar factorization and monotone rearrangement of vector-valued functions. *Comm. on Pure and Applied Math.*, 44:375–417, 1991.

[3] John Brothers and Frank Morgan. The isoperimetric theorem for general integrands. *Michigan Math. J.*, 41(3):419–431, 1994.

[4] Jaigyoung Choe. Every stationary polyhedral set in R^n is area minimizing under diffeomorphisms. *Pacific J. Math.*, 175(2):439–446, 1996.

[5] James Dilts. A metacalibration proof of the isoperimetric problem. *Rose-Hulman Undergrad. Math. J.*, 11(2):33–48, 2010.

[6] James Dilts, Rebecca Dorff, and Donald Sampson. A new proof of the double bubble conjecture in $\mathbb{R}^n$. *(In progress)*, 2011.

[7] R. Dorff, K. Fears, A. Stockman, and S. Uhl. Solving a combined Steiner and isoperimetric problem using metacalibration. 2008.

[8] R. Dorff, D. Johnson, G. Lawlor, and D. Sampson. Isopermimetric surfaces with boundary. *Proc. of the AMS*, 139:4467–4473, 2011.

[9] Rebecca Dorff and Donald Sampson et al. Proof of the planar double bubble conjecture using metacalibration methods. *Involve*, 2(5):611–628, 2009.

[10] Joel Foisy, Manuel Alfaro, Jeffrey Brock, Nickelous Hodges, and Jason Zimba. The standard double soap bubble in $\mathbf{R^2}$ uniquely minimizes perimeter. *Pacific J. Math*, 159:47–59, 1993.

[11] Michael Gromov. Isoperimetric inequalities in riemannian manifolds, Appendix I to Asymptotic Theory of Finite Dimensional Normed Spaces by Vitali D. Milman and Gideon Schechtman, Lecture Notes in Mathematics, No. 1200. Springer-Verlag, New York, 1986.

[12] Reese Harvey and H. Blaine Lawson Jr. Calibrated geometries. *Acta Mathematica*, 148(1):47–157, July 1982.

[13] Michael Hutchings, Frank Morgan, Manuel Ritoré, and Antonio Ros. Proof of the double bubble conjecture. *Annals of Math.*, 155:458–489, 2002.

[14] Cyril Isenburg. *The Science of Soap Films and Soap Bubbles*. Dover, 1992.

[15] Donald Sampson Jacob Ross and Neil Steinburg. Soap film realization of isoperimetric surfaces with boundary. *Involve*, In Press.

[16] Herbert Knothe. Contributions to the theory of convex bodies. *Michigan Math. J.*, (4):39–52, 1957.

[17] Gary Lawlor. Metacalibrations: Brief introduction. 2008. unpublished.

[18] Gary R. Lawlor and Frank Morgan. Paired calibrations applied to soap films, immiscible fluids, and surfaces or networks minimizing other norms. *Pacific J. Math.*, 166(1):55–83, 1994.

[19] Robert J. McCann. A convexity principle for interacting gases. *Adv. Math.*, 128:153–179, 1997.

[20] Frank Morgan. *Geometric Measure Theory: A beginner's guide*. Academic Press, 1988.

[21] John Oprea. *Differential Geometry and its Applications*. MAA, 2nd edition, 2007. Schmidt's proof of the isoperimetric inequality, p.39-42.

[22] Murry Rosenblatt. Remarks on a multivariate transformation. *Ann. Math. Statist.*, 23(3):470–472, 1952.

[23] Jean Taylor. The structure of singularities in soap-bubble-like and soap-film-like minimal surfaces. *Annals of Math.*, 103:489–539, 1976.